

---

# Learning to Segment for Vehicle Routing Problems

---

Wenbin Ouyang

MIT

oywenbin@mit.edu

Sirui Li

MIT

siruil@mit.edu

Yining Ma\*

MIT

yiningma@mit.edu

Cathy Wu

MIT

cathywu@mit.edu

## Abstract

Iterative search heuristics are widely recognized as state-of-the-art for solving Vehicle Routing Problems (VRPs). In this work, we identify and exploit a critical observation: within these solvers, a large portion of the solution remains stable, i.e., unchanged across search iterations, causing redundant computations, especially for large-scale VRPs with long subtours. To address this, we pioneer the formal study of the First-Segment-Then-Aggregate (FSTA) decomposition technique to accelerate iterative solvers. Specifically, FSTA preserves stable solution segments during the search, aggregates nodes within each segment into fixed hypernodes, and focuses the search only on unstable portions. Yet, a key challenge lies in identifying which segments should be aggregated by FSTA. To this end, we then introduce Learning-to-Segment (L2Seg), a novel neural framework to intelligently differentiate potentially stable and unstable portions for FSTA decomposition. We present three L2Seg variants: non-autoregressive (globally comprehensive but locally indiscriminate), autoregressive (locally refined but globally deficient), and their synergy, with bespoke training and inference strategies. Empirical results on CVRP and VRPTW suggest that L2Seg accelerates state-of-the-art iterative solvers by up to 7x. Additionally, we provide in-depth analysis showing NAR and AR synergy achieves best performance by combining their complementary strengths. Notably, L2Seg is a flexible framework that is compatible with traditional, learning-based, and hybrid solvers, while supporting a broad class of VRPs.

## 1 Introduction

Vehicle Routing Problems (VRPs) have profound applications such as in logistics and ride-hailing, driving decades of advances in combinatorial optimization [1]. As NP-hard problems, they are typically tackled with heuristics approximately. Neural Combinatorial Optimization (NCO) [2–6] has recently introduced machine learning into VRP solving, enabling data-driven decision-making with minimal domain knowledge while matching and even surpassing the performance of meticulously designed heuristics such as Lin-Kernighan-Helsgaun (LKH) [7] and Hybrid Genetic Search (HGS) [8].

Generally, state-of-the-art classic and neural VRP solvers predominantly rely on iterative search to refine the current best-so-far solution through local search (e.g., ruin and repair). However, as we observe in Section 3, a significant portion of edges *stabilize*, or their presence in the solution stops changing between iterations, as the search progresses, despite repeated local search computations. Specifically, we refer *stable edges* as those that consistently remain in the solution across iterations, while *unstable edges* are likely to be re-optimized. This is particularly evident in VRPs with long

---

\*Corresponding author.

subtours, where inner edges remain fixed while only boundary edges undergo frequent combinatorial changes. Intuitively, such stability can be inferred from the spatial distribution of customer nodes and the solution properties through end-to-end machine learning. Yet, existing solvers overlook such opportunities, leading to redundant computations that hinder their scalability and efficiency, especially in large-scale VRPs with long subtours.

Motivated by this critical observation, we study how learning to identify such *segments* can accelerate iterative search solvers, a perspective yet to be explored to the best of our knowledge. To this end, we formalize a **First-Segment-Then-Aggregate (FSTA)** decomposition framework, which identifies stable segments in a VRP solution and then aggregates them as fixed (one or two) hypernodes with combined attributes (e.g., total demand, min/max time windows). This not only decomposes the original large problem into more tractable subproblems but also significantly accelerates the search by leveraging iterative local search to strategically focus on unstable portions. We further show that FSTA preserves solution equivalence and is broadly applicable to VRPs with diverse constraints.

Yet, identifying unstable portions for effective FSTA decomposition remains a key challenge. We then introduce **Learning-to-Segment (L2Seg)**, a novel learning-guided framework that leverages deep models to intelligently differentiate potentially stable and unstable portions, allowing dynamic decomposition for accelerated local search. Realizing this, however, is nontrivial: it involves a large combinatorial decision space, requiring accurate segment grouping across optimization stages. Moreover, it demands modeling complex interdependencies among predicted edges, constraints, spatial distribution, solution structures, and both node and edge features.

To address these challenges, L2Seg considers a spatial locality strategy to restrict the search space and employs encoder-decoder-styled neural models. The encoder integrates graph-level and route-level features using attention and customized graph neural networks, generating node embeddings that guide edge re-optimization predictions in the decoder. L2Seg offers three decoder variants: (1) L2Seg-NAR (Non-Autoregressive): which features one-shot fast global prediction; (2) L2Seg-AR (Autoregressive), which enjoys sequential dependency modeling for high-precision local predictions; and (3) L2Seg-SYN (Synergized), which balances the strengths of NAR and AR for best performance. Notably, this represents a pioneering work that explores the joint decision-making between AR and NAR models in neural combinatorial optimization. Our L2Seg models are trained on datasets labeled using a lookahead procedure: edge stability is classified based on whether its presence in the solution was changed during re-optimization across the iterative search.

Through extensive experiments on large-scale CVRPs and VRPTWs, we show that L2Seg accelerates heuristics by 2x to 7x, enabling them to outperform various state-of-the-art traditional, neural, and hybrid baselines. Notably, L2Seg exhibits strong flexibility and generality in enhancing a wide range of backbone solvers, including traditional LKH-3 [7] solver, other orthogonal Large Neighborhood Search (LNS) framework [9], and recent learning-guided decomposition method Learning-to-Delegate (L2D) [4]. We further analyze the synergy between AR and NAR models in segment decision-making. Our analysis reveals the complementary strengths and weaknesses of NAR and AR models, and shows their synergy achieves best performance by integrating NAR’s global detection capability with AR’s local refinement precision.

Our contributions are as follows: (1) We make a critical yet underexplored insight that stable segments persist across search iterations in large-scale VRPs, causing redundant computations; (2) We formally study First-Segment-Then-Aggregate (FSTA), a generic decomposition framework that aggregates stable segments into fixed hypernodes while ensuring provable equivalence; (3) We propose Learning-to-Segment (L2Seg), a learning-guided framework with bespoke network architecture, training, and inference for identifying such segments; (4) We propose autoregressive, non-autoregressive, and their synergistic deep models, pioneering the first-of-its-kind study in NCO; (5) L2Seg consistently accelerates state-of-the-art iterative VRP solvers by 2x to 7x, boosting both traditional and learning-based solvers, including other decomposition frameworks. Our work presents a new perspective in NCO by introducing a segment-based acceleration framework that removes redundant search, achieves state-of-the-art on CVRP and VRPTW, while supporting a broad class of VRPs.

## 2 Related Works

**Existing VRP Solvers.** Classical VRP solvers include exact methods with guarantees [10] and practical heuristics [7]. Recently, inspired by Pointer Networks [11], machine learning has been

applied to combinatorial optimization, either end-to-end [2, 12–19] or following a learning-guided paradigm to inject data-driven insights into backbone optimizers [4, 20–24]. For VRPs, the former could yield competitive performance to classic methods [16, 25], while the latter often achieve state-of-the-art performance [4, 26]. Among these, most effective VRP solvers rely on iterative search, including classic heuristics such as HGS [8], LNS [9] and LKH [7]; neural solvers that learn local search [27–31]; neural constructive solvers integrated with search components [25, 32–37]; and hybrid learning-guided methods like L2D [4]. However, both handcrafted and neural iterative search solvers overlook the redundant computations identified in this paper, particularly in large-scale VRPs.

**Decomposition for Large-scale VRPs.** Scalability in VRP solvers often relies on effective decomposition [38]. Recently, machine learning has been leveraged to assist decomposition, such as sub-tour grouping [4, 39] and problem variant reduction [40, 41], or to boost neural solvers such as action space decomposition [16, 25, 42] and spatial-based decomposition [26, 43, 44]. In this paper, we present FSTA and L2seg, a fresh segment-based decomposition framework. Notably, L2Seg holds potential to enhance the other decomposition methods, such as LNS [9] and L2D [4]. While FSTA is conceptually related to path decomposition [38], which clusters nearby routes using barycenters, FSTA generalizes it by allowing segments of arbitrary length, reversals, and attribute aggregation. While another related work [45] explores segment stability for re-optimization in a specific dynamic CVRP setting, our work addresses a different problem, i.e., identifying stable segments across search steps to accelerate iterative solvers. And we formally analyze the nontrivial solution equivalence of FSTA across broader VRP variants. Moreover, L2Seg uniquely integrates three novel deep learning models (AR, NAR, and synergized) to dynamically guide FSTA decomposition during search.

**Autoregressive and Non-autoregressive Models.** In NCO, NAR models make fast, global predictions such as edge selection heatmaps [34, 40, 46] in a one-shot manner. However, they struggle to model complex interdependencies, particularly VRP constraints. In contrast, AR models make sequential predictions, one variable at a time, offering stronger modeling capacity but might overlook global structure. They excel in complex tasks, e.g., learning-to-construct (e.g., [25]) and learning-to-search solvers (e.g., [28]). Recent NCO works combine AR and NAR models in divide-and-conquer frameworks, with NAR for sub-problem splitting and AR for solving [26, 40, 41]. Other than task separation, we are the first to leverage their complementary strengths for joint decision-making, enabling more effective identification of unstable segments in FSTA decomposition.

### 3 First-Segment-Then-Aggregate (FSTA)

#### 3.1 Vehicle Routing Problems (VRPs)

VRPs aim to minimize total travel costs (often distance or travel time) while serving a set of customers under constraints. Formally, A VRP  $P$  is defined on a graph  $G = \{V, E\}$ , where each node  $x_i \in V$  represents a customer and each edge  $e_{i,j} \in E$  represents traveling from  $x_i$  to  $x_j$  and is associated with a travel cost. For Capacitated VRP (CVRP), vehicles of capacity  $C$  start and end at a depot node  $x_0$ . The sum of the demands  $d_i$  on any route must not exceed  $C$ , and each customer should be served exactly once. For VRP with Time Windows (VRPTW), each customer is additionally associated with a service time  $s_i$  and a time window  $[t_i^l, t_i^r]$  within which service must begin.

#### 3.2 FSTA Decomposition

Figure 1 depicts that iterative search solvers perform *redundant searches*, reoptimizing only a small portion while many edges remain unchanged, especially in large subtours with high capacity  $C$ . More visualization are provided in Appendix A.1. Inspired by [45], we formally study the decomposition technique, First-Segment-Then-Aggregate (FSTA), for accelerating iterative search solvers. As shown in the top of Figure 2, FSTA

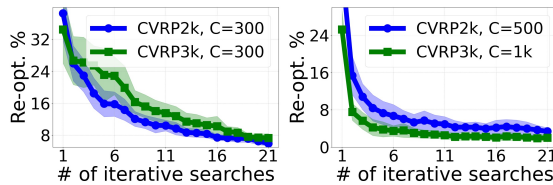


Figure 1: Percentage of re-optimized edges during iterative search process: using LKH-3 on 100 CVRP instances of sizes 2k and 3k with large and small  $C$ . A vast majority of edges remain unchanged, suggesting redundant calculations.

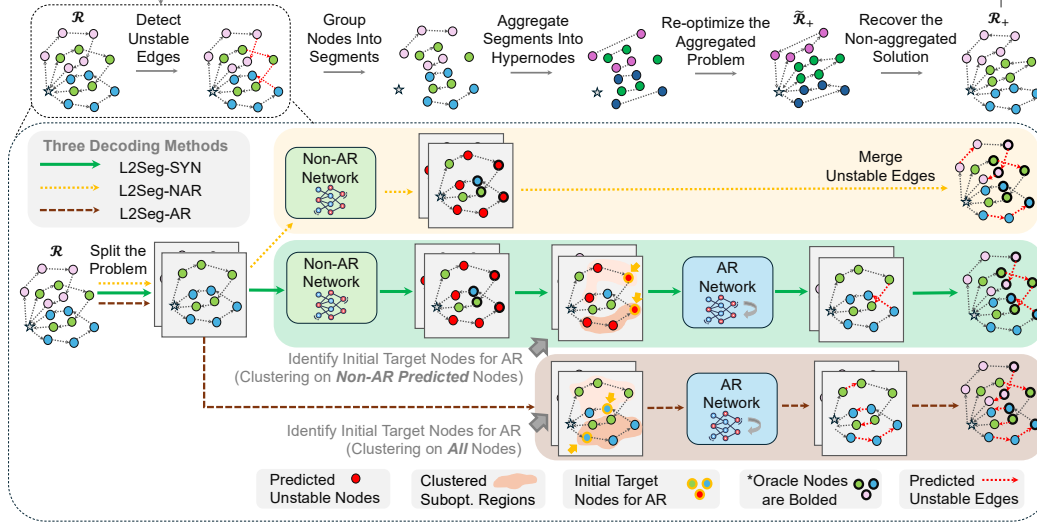


Figure 2: The overview of our FSTA decomposition framework (top) and the three proposed L2Seg models (bottom). L2Seg-SYN employs a four-step synergized approach: (1) problem decomposition into subproblems, (2) unstable nodes detection globally via NAR decoding, (3) clustering of NAR-predicted nodes to localize unstable regions and select initial target nodes, and (4) refining unstable edge predictions locally via AR decoding starting from these identified initial target nodes.

segments the VRP solutions by identifying unstable portions, and then groups them into hypernodes with aggregated attributes. We thus expect more efficient re-optimization on the reduced problems.

**Segment Definition.** Denote the solution (set of routes) of a CVRP as  $\mathcal{R} = \{R^1, R^2, \dots\}$ , and each route as  $R^i = (x_0 \rightarrow x_1^i \rightarrow x_2^i \rightarrow \dots \rightarrow x_0) \in \mathcal{R}$ , where the first and the last nodes in  $R^i$  are the depot. A segment consists of some consecutive nodes within a route. We denote the segment containing the  $j^{\text{th}}$  to  $k^{\text{th}}$  nodes of route  $i$  as  $S_{j,k}^i = (x_j^i \rightarrow \dots \rightarrow x_k^i)$ . An aggregated segment  $\tilde{S}_{j,k}^i$  uses one hypernode ( $\tilde{S}_{j,k}^i = \{\tilde{x}_{j,k}^i\}$ ) or two hypernodes ( $\tilde{S}_{j,k}^i = \{\tilde{x}_j^i, \tilde{x}_k^i\}$ ) with aggregated attributes (e.g. the demand of  $\tilde{x}_{j,k}^i$  equals to  $d_j^i + \dots + d_k^i$ ) to represent the non-aggregated segment  $S_{j,k}^i$ .

**FSTA Solution Update.** After identifying unstable edges  $\{e_{j_1}^i, e_{j_2}^i, \dots\}$  in each route (which will be addressed in Section 4), where each  $e_j^i$  denotes the edge starting from the  $j^{\text{th}}$  node in route  $R^i$ , we break these edges and group the remaining stable edges into segments. To preserve a valid depot, edges connecting to the depot are included in the unstable edge set. After unstable edges are removed, each route  $R^i$  is then decomposed into multiple disjoint segments  $\{x_0, S_{1,j_1}^i, S_{j_1,j_2}^i, \dots\}$ , where  $x_0$  is depot. Each segment  $S_{j,k}^i$  is then aggregated into one or two hypernodes  $\tilde{S}_{j,k}^i$ , leading to a reduced problem  $\tilde{P}$ . We then obtain the corresponding solution  $\tilde{\mathcal{R}}$  for such reduced problem, where for each  $\tilde{R}^i \in \tilde{\mathcal{R}}$ , we have  $\tilde{R}^i = (x_0 \rightarrow \tilde{S}_{1,j_1}^i \rightarrow \tilde{S}_{j_1,j_2}^i, \dots \rightarrow x_0)$ . With fewer nodes than the original problem  $P$ , re-optimization with a backbone solver becomes more efficient, which is analyzed and confirmed in Appendix A.1. After re-optimization, we obtain a new solution  $\tilde{\mathcal{R}}_+$  for the reduced problem  $\tilde{P}$ , which is then recovered into a solution  $\mathcal{R}_+$  for the original problem  $P$  by expanding each hypernode(s) back into its original segment of nodes. This relies on our monotonicity theorem, which guarantees that an improved solution in  $\tilde{P}$  maps to an improved solution in  $P$ .

**Theoretical Analysis.** We establish a theorem proving FSTA decomposition’s feasibility and monotonicity across multiple VRP variants (e.g. CVRP, CVRPTW), with the proof in Appendix A.2.

**Theorem (Feasibility & Monotonicity).** If the aggregated solution  $\tilde{\mathcal{R}}_+$  is feasible to the aggregated problem, then  $\mathcal{R}_+$  is also feasible to the original, non-aggregated problem.

Moreover, if two feasible aggregated solutions  $\tilde{\mathcal{R}}_+^1$  and  $\tilde{\mathcal{R}}_+^2$  satisfy  $f(\tilde{\mathcal{R}}_+^1) \leq f(\tilde{\mathcal{R}}_+^2)$ , where  $f(\cdot)$  denotes the objective function (total travel cost), their corresponding original solutions also preserve this order:  $f(\mathcal{R}_+^1) \leq f(\mathcal{R}_+^2)$ .



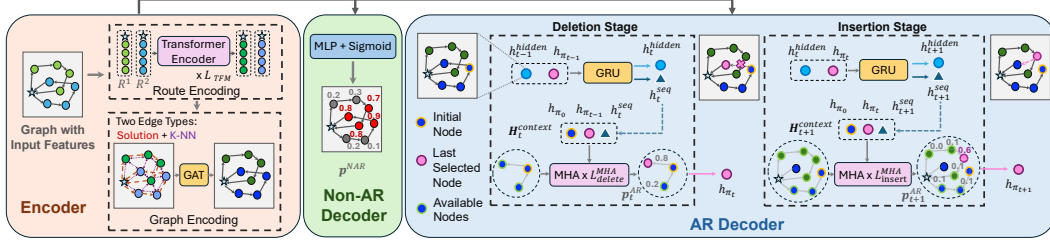


Figure 3: Architecture of L2Seg: encoder (left), NAR decoder (center), and AR decoder (right). NAR predicts unstable nodes for associated edges. AR uses a two-stage process, where the insertion bridges the deletion stage to accurately detect unstable edges locally, akin to the local search behavior.

## 4 Learning to Segment (L2Seg)

Effective FSTA decomposition requires accurate identification of stable and unstable edges in solution  $\mathcal{R}$ . In this section, we introduce **Learning to Segment (L2Seg)**, a neural framework for predicting unstable edges to guide FSTA. There are two natural paradigms: 1) Non-autoregressive (NAR) and 2) Autoregressive (AR) models. *NAR models*, e.g., heatmap, offer global predictions with an efficient single forward pass. However, they lack conditional modeling to accurately capture local dependencies. For example, when one edge is unstable, nearby edges often show instability, though not all are unstable. NAR models may fail to distinguish them and tend to mark all neighboring edges as unstable. On the other hand, *AR models*, e.g., attention-based models, can more natively capture local dependencies. Yet, they may miss the crucial global structure. For example, when unstable edges are distributed across distant regions, AR models may struggle to recognize and model these broader patterns. Our approach offers three variants as shown in Figure 2: non-autoregressive (L2Seg-NAR), autoregressive (L2Seg-AR), and a synergized combination of both (L2Seg-SYN).

### 4.1 Neural Architecture

The autoregressive and non-autoregressive models of L2Seg share the same encoder structure. Next, we first describe the encoder, and then the two decoder architectures.

**Input Feature Design.** We propose enhanced input features for L2Seg to better distinguish unstable and stable edges (see Appendix A.1 for intuitions). Key features include node angularity relative to the depot and node internality, where the latter measures the proportion of nearest nodes within the same route. We consider two edge types: edges in the current solution  $\mathcal{R}$  and edges connecting each node to their  $k$ -nearest neighbors. Appendix B.1 provides a detailed feature description.

**Encoder.** Given node features  $\mathbf{X} = (\mathbf{x}_0, \mathbf{x}_1, \dots)$  and edge features  $\mathbf{E} = \{\mathbf{e}_{0,1}, \mathbf{e}_{0,2}, \dots\}$ , we compute the initial node embedding as  $\mathbf{h}_i^{\text{init}} = \text{Concat}(\mathbf{h}_i^{\text{MLP}}, \mathbf{h}_i^{\text{POS}}) \in \mathbb{R}^{2d_h}$ , where  $\mathbf{h}_i^{\text{MLP}}$  and  $\mathbf{h}_i^{\text{POS}}$  are obtained by passing  $\mathbf{x}_i$  through a multilayer perceptron (MLP) and an absolute position encoder [47], respectively. Next, we process the embeddings using  $L_{\text{TFM}}$  Transformer layers [47] with masks to prevent computation between nodes in different routes:  $\mathbf{h}_i^{\text{TFM}} = \text{TFM}(\mathbf{h}_i^{\text{init}}) \in \mathbb{R}^{d_h}$ . This step encodes local structural information from the current solution. Finally, we compute the node embeddings  $\mathbf{H}^{\text{GNN}} = \{\mathbf{h}_i^{\text{GNN}} \in \mathbb{R}^{d_h} \mid i = 0, \dots, |V|\}$  leveraging the global graph information by using  $L_{\text{GNN}}$  layers of a Graph Attention Network (GAT) [48], where  $\mathbf{H}^{\text{GNN}} = \text{GNN}(\mathbf{H}^{\text{TFM}}, \mathbf{E})$ .

**Non-Autoregressive Decoder.** It uses an MLP with a sigmoid function to decode the probability  $\mathbf{p}^{\text{NAR}}$  of each node being unstable globally in one shot, so as to identify associated unstable edges:

$$\mathbf{p}^{\text{NAR}} = \text{MLP}_{\text{NAR}}(\mathbf{H}^{\text{GNN}}) \quad (1)$$

**Autoregressive Decoder.** To model the interdependence of unstable edges, the autoregressive decoder generates the unstable edge set sequentially following a sequence  $a = \{x_{\pi_0}, x_{\pi_1}, \dots\}$ . Motivated by classical local search where  $k$  removed unstable edges are linked via  $k$  newly inserted edges between their endpoints [28, 49], this sequence is generated by alternating between a deletion stage that identifies unstable edges and an insertion stage that introduces a pseudo-edge to more accurately bridge to the next unstable edge, ending when a special token  $x_{\text{end}}$  is selected. Note that the insertion stage does not add new edges to the solution; it solely models the interdependence of consecutive

unstable edges, reflecting the local search principle that removed edges are typically reconnectable via new insertions. Formally, denote the set of edges within the current solution as  $E_{\mathcal{R}}$ . The decoding alternates between: (1) **Deletion** ( $t = 2k$ ): Selects an unstable edge  $e_{\pi_{2k}, \pi_{2k+1}} \in E_{\mathcal{R}}$  based on a target node, which is either initialized at the first step (see Section 4.3) or the one obtained from the previous insertion step; one of the two edges connected to this node in the current solution is then selected as unstable (more than two candidates may exist if the node is the depot); and (2) **Insertion** ( $t = 2k + 1$ ): Selects a new edge  $e_{\pi_{2k+1}, \pi_{2k+2}} \notin E_{\mathcal{R}}$  that links to the endpoint of the last unstable edge removed, exploring  $O(|V|)$  potential candidates to serve as a bridge to the next unstable target node (next unstable region). From  $a$ , we then identify the set of removed edges as the unstable edges, i.e.,  $E_{\text{unstable}} = \{e_{\pi_0, \pi_1}, e_{\pi_2, \pi_3}, \dots\}$ . Both stages employ two principal modules: Gated Recurrent Units (GRUs) [50] to encode sequence context, and multi-head attention (MHA) [47] for node selection. The GRU’s initial hidden state is the average of all node embeddings:  $\mathbf{h}_0^{\text{hidden}} = \frac{1}{|V|} \sum_{i=0}^{|V|} \mathbf{h}_i^{\text{GNN}}$ . At step  $t$ , the sequence embedding is updated by  $\mathbf{h}_t^{\text{seq}} = \text{GRU}(\mathbf{h}_{t-1}^{\text{hidden}}, \mathbf{h}_{\pi_{t-1}}^{\text{GNN}})$ , and the context embedding is formed by concatenating the embeddings of the initial node, the previous node, and the new sequence embedding:  $\mathbf{H}_t^{\text{context}} = \text{Concat}(\mathbf{h}_{\pi_0}^{\text{GNN}}, \mathbf{h}_{\pi_{t-1}}^{\text{GNN}}, \mathbf{h}_t^{\text{seq}})$ .

Inspired by the decoder design in LEHD [25], we use two distinct MHA modules with  $L^{\text{MHA}}$  layers, to decode  $x_{\pi_t}$ . Specifically, considering the size of the action space (at most 2 for deletion and  $O(|V|)$  for insertion), we utilize a shallow decoder ( $L_{\text{delete}}^{\text{MHA}} = 1$ ) during the deletion stage and a deeper decoder ( $L_{\text{insert}}^{\text{MHA}} = 4$ ) during the insertion stage. Let  $\mathbf{H}_t^a \subseteq \mathbf{H}^{\text{GNN}}$  denote the set of available nodes at step  $t$ . During the insertion stage, we also incorporate an additional candidate  $\mathbf{h}^{\text{end}} = \alpha \mathbf{h}_{\pi_0}^{\text{GNN}} + (1 - \alpha) \frac{1}{|V|} \sum_{i=0}^{|V|} \mathbf{h}_i^{\text{GNN}}$ , where  $\alpha$  is a learnable parameter, to indicate termination of decoding, providing the AR model with the flexibility to determine the number of unstable edges. Formally, the decoding at step  $t$  is given as follows; note that the first 3 dimensions of  $\mathbf{H}^{(L^{\text{MHA}})}$  corresponds to the context embeddings  $\mathbf{H}_t^{\text{context}}$  and hence are masked from selection:

$$\begin{aligned} \mathbf{H}^{(0)} &= \text{Concat}(\mathbf{H}_t^{\text{context}}, \mathbf{H}_t^a), \mathbf{H}^{(l)} = \text{MHA}(\mathbf{H}^{(l-1)}), \\ u_i &= \begin{cases} (W_q \mathbf{h}^c)^T W_k \mathbf{h}_i^{(L^{\text{MHA}})} / \sqrt{d_h}, & \text{if } i > 3, \\ -\infty, & \text{otherwise,} \end{cases} \end{aligned} \quad (2)$$

where  $1 \leq l \leq L^{\text{MHA}}$ ,  $W_q$  and  $W_k$  are learnable matrices, and  $\mathbf{h}^c \in \mathbb{R}^{6d_h}$  concatenates the first three columns of  $\mathbf{H}^{(0)}$  and  $\mathbf{H}^{(L^{\text{MHA}})}$  along the last axis. The node  $x_{\pi_t}$  is sampled from  $\mathbf{p}_t^{\text{AR}} = \text{softmax}(\mathbf{u})$ .

## 4.2 Training

We employ iterative solvers as look-ahead heuristics to detect unstable edges. We then utilize imitation learning to train L2Seg models, so as to replicate the behavior of the look-ahead heuristics.

**Dataset Construction.** Let the edges indicated by a solution  $\mathcal{R}$  be  $E_{\mathcal{R}}$ , and the nodes indicated by an edge set  $E$  be  $V_E$ . Given  $P$  with the current solution  $\mathcal{R}$ , we first employ an iterative solver  $\mathcal{S}$  to refine  $\mathcal{R}$  and obtain  $\mathcal{R}_+$ . We then collect the differing edges between  $\mathcal{R}$  and  $\mathcal{R}_+$  as  $E_{\text{diff}} = (E_{\mathcal{R}} \setminus E_{\mathcal{R}_+}) \cup (E_{\mathcal{R}_+} \setminus E_{\mathcal{R}})$  (including both the deleted and newly inserted edges). Next, we identify the set of unstable nodes  $V_{\text{unstable}} = V_{E_{\text{diff}}}$ , i.e., the set of nodes that are end points to some edge in  $E_{\text{diff}}$ . We empirically observe that solution refinement typically takes place between two adjacent routes. **For the NAR model**, we construct a dataset with binary labels. Each problem-label pair consists of a decomposed problem containing two adjacent routes and binary labels indicating whether each node is unstable (1) or stable (0). Formally, a node  $x$  is labeled 1 if  $x \in V_{\text{unstable}}$ .

To capture local dependencies among unstable edges, we construct AR labels as node sequences that preserve these relationships. Nodes without local dependencies are naturally excluded through connected component partitioning. We thus obtain the set of connected components  $\mathcal{K}$  induced by  $E_{\text{diff}}$  and select those containing nodes from at most two routes, denoted by  $\mathcal{K}_{\text{TR}}$ . For all  $K \in \mathcal{K}_{\text{TR}}$ , let  $R_i$  and  $R_j$  be the two routes ( $\forall x \in K, x \in R_i \cup R_j$ ). We then form a subproblem  $P_K$  containing those two routes with solution  $\mathcal{R}_K = \{R_i, R_j\}$ . For any  $K \in \mathcal{K}_{\text{TR}}$ , we extract a sequence of nodes  $y_K = \{x_{\pi_0}, x_{\pi_1}, \dots, x_{\pi_m}, x_{\text{end}}\}$  as the label for the AR model (alternatively deleting and inserting edges). With the corresponding problem  $P_K$ , we construct problem-label pairs with the corresponding  $y_K$  **for the AR model**. Additional details are in Appendix C.5..

**Loss Function.** To balance labels, we use weighted binary cross-entropy for the NAR model ( $w_{\text{pos}} > 1$ ) and weighted cross-entropy for the AR model to balance the two stages ( $w_{\text{insert}} > w_{\text{delete}}$ ).

$$L_{\text{NAR}}(\mathbf{p}^{\text{NAR}}, y^{ij}) = - \sum_{y_{x_k} \in y^{ij}} w_{\text{pos}} y_{x_k} \log(p_k^{\text{NAR}}) + (1 - y_{x_k}) \log(1 - p_k^{\text{NAR}})$$

$$L_{\text{AR}}(\mathbf{p}^{\text{AR}}, y_K) = - \sum_{x_{\pi_{2k}} \in y_K} w_{\text{insert}} \log(p_{\pi_{2k}}^{\text{AR}}) - \sum_{x_{\pi_{2k+1}} \in y_K} w_{\text{delete}} \log(p_{\pi_{2k+1}}^{\text{AR}}).$$

### 4.3 Inference

We describe the synergized inference that combines the benefits of global structural awareness from NAR with the local precision from AR, followed by two simpler variants using only NAR or AR.

**Synergized Prediction (L2Seg-SYN).** L2Seg-SYN’s inference pipeline for detecting unstable edges consists of four steps: (1) problem decomposition, (2) global unstable node detection via NAR decoding, (3) representative initial node identification for AR decoding based on NAR predictions, and (4) local unstable edge detection using AR decoding.

Given a problem  $P$  with solution  $\mathcal{R}$ , we partition  $P$  into approximately  $|\mathcal{R}|$  subproblems,  $\mathcal{P}_{\text{TR}}$ , by grouping nodes from all two adjacent sub-tour pairs. For each subproblem in  $\mathcal{P}_{\text{TR}}$ , the NAR model predicts unstable nodes as  $\hat{y}_{\text{NAR}} = \{x_i \mid p_i^{\text{NAR}} \geq \eta\}$ , where  $\eta$  is a predefined threshold. We then refine unstable edge detection with the AR model within regions identified by the NAR prediction. To reduce redundant decoding efforts on neighboring unstable nodes, we first group unstable nodes into  $n_{\text{KMEANS}}$  clusters using the  $K$ -means algorithm, and select the node with the highest  $p_i^{\text{NAR}}$  within each cluster as the starting point for AR decoding. The AR model then detects unstable edges based on these initial nodes. Finally, we aggregate unstable edges from all subproblems in  $\mathcal{P}_{\text{TR}}$  as the final unstable edge set for  $P$  given the current solution  $\mathcal{R}$ .

**Non-Autoregressive Prediction (L2Seg-NAR).** L2Seg-NAR uses only the NAR model for predictions. It identifies unstable nodes and marks all connected edges as unstable.

**Autoregressive Prediction (L2Seg-AR).** Unlike L2Seg-SYN, L2Seg-AR exclusively utilizes the AR model. Instead of using the NAR model to detect unstable nodes, it assumes all nodes may be unstable, hence applying the  $K$ -means algorithm on all nodes. It then selects the node closest to each cluster center as the initial node for AR-based decoding.

## 5 Experiment

Our decomposition-based FSTA and L2Seg excel on large-scale problems. In this section, we first evaluate how L2Seg-AR, L2Seg-NAR, and L2Seg-SYN accelerate various learning and non-learning iterative solvers on large-capacity CVRPs with long subtours. Next, we compare L2Seg against state-of-the-art baselines on standard benchmark CVRP and VRPTW instances. Finally, we provide in-depth analyses of our pipeline. Additional results and discussions are available in Appendix D. Our code, pre-trained models, and the dataset will be released on Github (see Appendix E).

**Backbone Solvers.** We integrate L2Seg with three representative backbones: LKH-3 [7] (*classic heuristic*), LNS [9] (*decomposition framework*), and L2D [4] (*learning-guided hybrid solvers*) to demonstrate the broad applicability of L2Seg. Details on backbones are provided in Appendix C.1.

**Baselines.** We include state-of-the-art classic solvers (LKH-3 [7], HGS [8]), neural solvers (BQ [16], LEHD [25], ELG [15], ICAM [51], L2R [42], SIL [5]), and learning-based divide-and-conquer methods (GLOP [40], TAM [41], UDC [26], L2D [4]). We rerun LKH-3, LNS, and L2D, and report results from [5, 26] for other baselines using the same benchmarks. See Appendix C.2 for details.

**Data Distribution.** We generate all training and test instances following prior works by Zheng et al. [26] for CVRP and Solomon [52] for VRPTW. See Appendix C.3 for details. For Section 5.1, results are averaged over 100 large-scale CVRP test instances at 2k and 5k scales (capacities 500 and 1,000, respectively). For Section 5.2, we follow standard NCO benchmarks, reporting averaged results on 1k, 2k, and 5k test datasets with 1,000 CVRP and 100 VRPTW instances per scale.

**Evaluation and Metric.** For all methods, we impose time limits of 150s, 240s, and 300s for CVRP1k, CVRP2k, and CVRP5k, and 120s, 240s, and 600s for VRPTW1k, VRPTW2k and VRPTW5k. Note

that each solver may finish a few seconds ( $< 10s$ ) beyond its limit. We set  $\eta = 0.6$  and  $n_{\text{KMEANS}} = 3$  for our L2Seg. Additional parameters are listed in Appendix C.4. We report travel cost and per-instance solve time for all cases, and report percentage improvements over backbone solvers in Section 5.1 and gaps to HGS (the best heuristic solvers) for both CVRP and VRPTW in Section 5.2.

### 5.1 L2Seg Accelerates Various Iterative Backbone Solvers

We first verify the effectiveness of the three proposed L2Seg variants to enhance backbone iterative solvers. Table 1 presents results on large-capacity, uniformly distributed CVRPs with long subtours. Results show that all L2Seg variants consistently improve each backbone solver across all problem scales. We also note that performance gains are larger for weaker backbones, and while L2Seg-AR and L2Seg-NAR each boost performance, their combination (L2Seg-SYN) delivers the best solutions. Figure 4 plots average objective curves over time, which reveals 2x to 7x speedups on the backbone iterative solvers with L2Seg-SYN. Remarkably, L2Seg-augmentation lets weaker solvers surpass stronger ones (e.g., LKH-3 + L2Seg-SYN outperforms vanilla LNS).

### 5.2 L2Seg Outperforms Both Classic and Neural Baselines on CVRP and VRPTW

We evaluate the highest-performing L2Seg-SYN implementation with three distinct backbone solvers and compare against state-of-the-art classical and neural approaches. As demonstrated in Table 2, L2Seg surpasses both classical and neural baselines on CVRP and VRPTW benchmarks. For CVRP, L2Seg achieves superior performance within comparable computational time relative to competitive classical solvers, including HGS on larger problem instances. It also outperforms the state-of-the-art learning-based constructive solver SIL [5] and divide-and-conquer solver L2D [4] across all problem scales. For VRPTW, L2Seg exceeds all classical and learning-based solvers by at least 3% across various scales under identical time constraints, with performance advantages increasing as problem size grows. Notably, L2Seg consistently enhances performance when integrated with any backbone solver, demonstrating its versatility. Additional analyses are provided in Appendix C.

### 5.3 Further Analysis and Discussions

**Ablation Study.** Table 3 compares the LNS backbone; random FSTA with 40% and 60% of edges arbitrarily marked as unstable; L2Seg-SYN w/o enhanced features; and full L2Seg-SYN. Results show that Random FSTA worsens performance; and only full L2Seg-SYN with enhanced features achieves top performance. This confirms that L2Seg’s learnable, feature-guided segmentation is indispensable for preserving high-quality segments in FSTA for boosting backbone solvers.

Table 1: Performance comparisons of our proposed L2Seg-NAR, L2Seg-AR, and L2Seg-SYN when accelerating three backbone solvers, LKH-3, LNS, and L2D, on the *large-capacity* CVRP instances. We report the objective value, improvement gain (%), and the time. The gains (the higher the better) are w.r.t. the performance of each backbone solver. Time limits were set to be 150s for CVRP2k and 240s for CVRP5k, respectively.

Methods	CVRP2k			CVRP5k		
	Obj.↓	Gain↑	Time↓	Obj.↓	Gain↑	Time↓
LKH-3 [7]	45.24	0.00%	152s	65.34	0.00%	242s
L2Seg-NAR-LKH-3	44.34	1.99%	158s	64.72	0.95%	246s
L2Seg-AR-LKH-3	44.23	2.23%	151s	64.67	1.03%	244s
<b>L2Seg-SYN-LKH-3</b>	<b>43.92</b>	<b>2.92%</b>	152s	<b>64.12</b>	<b>1.87%</b>	248s
LNS [9]	44.92	0.00%	154s	64.69	0.00%	246s
L2Seg-NAR-LNS	44.12	1.78%	154s	64.38	0.48%	244s
L2Seg-AR-LNS	44.02	2.00%	157s	64.24	0.70%	249s
<b>L2Seg-SYN-LNS</b>	<b>43.42</b>	<b>3.34%</b>	152s	<b>63.94</b>	<b>1.16%</b>	241s
L2D [4]	43.69	0.00%	153s	64.21	0.00%	243s
L2Seg-NAR-L2D	43.55	0.32%	152s	64.02	0.30%	243s
L2Seg-AR-L2D	43.53	0.37%	156s	64.12	0.14%	247s
<b>L2Seg-SYN-L2D</b>	<b>43.35</b>	<b>0.78%</b>	157s	<b>63.89</b>	<b>0.50%</b>	248s

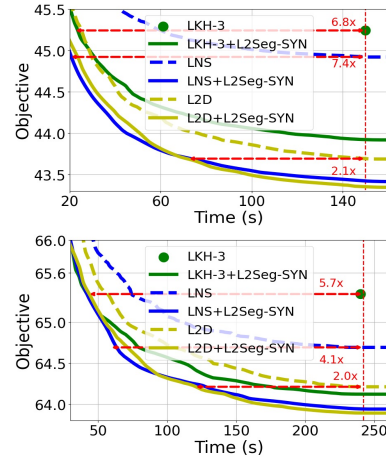


Figure 4: Search curves for L2Seg on three backbone solvers on large capacity CVRP2k (upper) and CVRP5k (lower). L2Seg achieves up to 7x speedups.

Table 2: Performance comparisons of our L2Seg-SYN-L2D against baselines on *benchmark* CVRP and VRPTW instances. The gap % (lower the better) is w.r.t. the performance of HGS.

Methods	CVRP1k			CVRP2k			CVRP5k		
	Obj.↓	Gap↓	Time↓	Obj.↓	Gap↓	Time↓	Obj.↓	Gap↓	Time↓
HGS [8]	41.20	0.00%	5m	57.20	0.00%	5m	126.20	0.00%	5m
LKH-3 [7]	42.98	4.32%	6.6m	57.94	1.29%	11.4m	175.70	39.22%	2.5m
LNS [9]	42.44	3.01%	2.5m	57.62	0.73%	4.0m	126.58	0.30%	5.0m
BQ [16]	44.17	7.21%	55s	62.59	9.42%	3m	139.80	10.78%	45m
LEHD [25]	43.96	6.70%	1.3m	61.58	7.66%	9.5m	138.20	9.51%	3h
ELG [15]	43.58	5.78%	15.6m	-	-	-	-	-	-
ICAM [51]	43.07	4.54%	26s	61.34	7.24%	3.7m	136.90	8.48%	50m
L2R [42]	44.20	7.28%	34.2s	-	-	-	131.10	3.88%	1.8m
SIL [5]	42.00	1.94%	1.3m	57.10	-0.17%	2.4m	123.10	-2.52%	5.9m
TAM(LKH-3) [41]	46.30	12.38%	4m	64.80	13.29%	9.6m	144.60	14.58%	35m
GLOP-G(LKH-3) [40]	45.90	11.41%	2m	63.02	10.52%	2.5m	140.40	11.25%	8m
UDC [26]	43.00	4.37%	1.2h	60.01	4.9%	2.15h	136.70	8.32%	16m
L2D [4]	42.07	2.11%	2.5m	57.44	0.42%	4.2m	126.48	0.22%	5.3m
L2Seg-SYN-LKH-3	41.42	0.53%	2.5m	56.37	-1.45%	4.4m	122.34	-3.16%	5.1m
L2Seg-SYN-LNS	41.36	0.39%	2.5m	56.08	-1.96%	4.1ms	121.96	-3.48%	5.1m
<b>L2Seg-SYN-L2D</b>	<b>41.23</b>	<b>0.07%</b>	2.5m	<b>56.05</b>	<b>-2.01%</b>	4.1m	<b>121.87</b>	<b>-3.55%</b>	5.1m

Methods	VRPTW1k			VRPTW2k			VRPTW5k		
	Obj.↓	Gap↓	Time↓	Obj. ↓	Gap↓	Time↓	Obj.↓	Gap ↓	Time↓
HGS [8]	90.35	0.00%	2m	173.46	0.00%	4m	344.2	0.00%	10m
LKH-3 [7]	91.32	1.07%	2m	174.25	0.46%	4m	353.2	2.61%	10m
LNS [9]	88.12	-2.47%	2m	165.42	-4.64%	4m	338.5	-1.66%	10m
L2D [4]	88.01	-2.59%	2m	164.12	-5.38%	4m	335.2	-2.61%	10m
L2Seg-SYN-LKH-3	88.65	-1.88%	2m	169.24	-2.43%	4m	345.2	0.29%	10m
L2Seg-SYN-LNS	87.31	-3.36%	2m	163.94	-5.49%	4m	334.1	-2.93%	10m
<b>L2Seg-SYN-L2D</b>	<b>87.25</b>	<b>-3.43%</b>	2m	<b>163.74</b>	<b>-5.60%</b>	4m	<b>333.4</b>	<b>-3.14%</b>	10m

Table 3: Performance of L2Seg-SYN v.s. Random FSTA to accelerate LNS on CVRP instances.

Methods	LNS (Backbone)	Random FSTA (40%)	Random FSTA (60%)	L2Seg-SYN w/o Enhanced Features	<b>L2Seg-SYN</b>
CVRP2k	44.92	46.24	46.89	43.65	<b>43.42</b>
CVRP5k	64.69	66.72	65.92	64.22	<b>63.94</b>

#### Why NAR+AR Is The Best Performance? We

offer the following insights: L2Seg-NAR effectively identifies unstable regions but lacks the ability to model dependencies among unstable edges, often over-classifying within these regions. L2Seg-AR captures local dependencies but struggles to detect unstable regions initially. L2Seg-SYN combines these strengths, identifying unstable regions through its NAR component and refining predictions via its AR component. We provide a conceptual illustration in Figure 5, with actual instance visualizations in Appendix D. Table 4 presents results on CVRP2k, where 16.4% of edges are unstable. Higher Recall enables more edges to be reoptimized, potentially improving solution quality, while higher TNR reduces problem size and runtime. L2Seg-NAR yields higher Recall but lower TNR, leading to longer runtimes. L2Seg-AR underperforms in both metrics, confirming its difficulty in identifying unstable regions.

**Pursuing High Recall v.s. High TNR.** Higher Recalls allow more unstable edges to be reoptimized, potentially improving solution quality, while higher TNRs reduce problem size and runtime. However, due to imprecision in learning, pursuing high TNRs often reduces Recall, causing premature convergence to local optima. Figure 6(b) shows that fixing too few edges (left: high Recall, low TNR) or too many (right: high TNR, low Recall) degrades performance. Our configuration (middle) balances this trade-off for optimal performance.

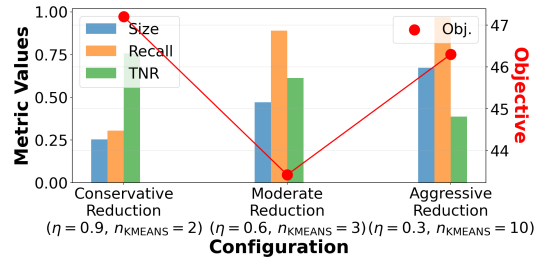


Figure 6: Problem size reduction and prediction statistics across L2Seg configurations (different problem reduction strategies). Size represents the ratio of reduced to original problem dimensions.

Table 4: Model prediction analysis of L2Seg-LNS on CVRP2k.

Methods	Recall $\uparrow$	TNR $\uparrow$	Obj. $\downarrow$
L2Seg-SYN	89.02%	<b>61.24%</b>	<b>43.42</b>
L2Seg-NAR	<b>91.46%</b>	51.79%	44.02
L2Seg-AR	74.39%	54.07%	44.12

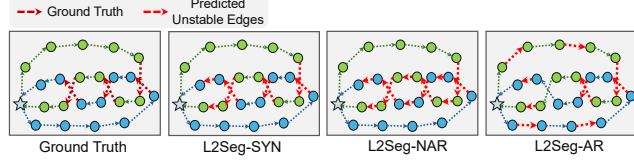


Figure 5: Illustration of L2Seg model behaviors.

## 6 Conclusion

This work introduces Learning-to-Segment (L2Seg), a novel learning-guided framework that accelerates state-of-the-art iterative solvers for large-scale VRPs by up to 7x. We first formalize the FSTA decomposition and then employ a specialized encoder-decoder architecture to dynamically differentiate potentially unstable and stable segments in FSTA. L2Seg features three model variants, L2Seg-NAR, L2Seg-AR, and L2Seg-SYN, pioneering the synergy of AR and NAR models in NCO. Extensive results show that L2Seg demonstrates state-of-the-art performance on representative CVRP and VRPTW and also exhibits flexibility in boosting traditional and learning-based solvers, including other decomposition frameworks. One potential limitation is that L2Seg is not guaranteed to boost all VRP solvers across all VRP variants. Future work includes: (1) extending L2Seg to accelerate a broader range of VRP solvers (e.g., [8, 53]); (2) applying L2Seg to additional VRP variants and other combinatorial optimization problems; (3) expanding the synergy between AR and NAR models to the broader NCO community; (4) distilling learned behavior via Large Language Models (LLMs) [54]; and (5) exploring the explainability and theoretical foundations of the learned behavior.

## Acknowledgments and Disclosure of Funding

This research was supported by a gift from Mathworks, as well as partial support from the MIT Amazon Science Hub, the National Science Foundation (NSF) award 2149548 and CAREER award 2239566, and an Amazon Robotics Fellowship. The authors acknowledge the MIT SuperCloud and Lincoln Laboratory Supercomputing Center for providing the high-performance computing resources that contributed to the research results reported in this paper. We particularly thank Andrea Lodi for the insightful discussions throughout this project, especially during its initial stages. We also thank Zhongxia "Zee" Yan, Jianan Zhou, and Samitha Samaranayake for their valuable input.

## References

- [1] Gilbert Laporte. Fifty years of vehicle routing. *Transportation science*, 43(4):408–416, 2009.
- [2] Wouter Kool, Herke van Hoof, and Max Welling. Attention, learn to solve routing problems! In *International Conference on Learning Representations*, 2018.
- [3] Yoshua Bengio, Andrea Lodi, and Antoine Prouvost. Machine learning for combinatorial optimization: a methodological tour d’horizon. *European Journal of Operational Research*, 290(2):405–421, 2021.
- [4] Sirui Li, Zhongxia Yan, and Cathy Wu. Learning to delegate for large-scale vehicle routing. *Advances in Neural Information Processing Systems*, 34:26198–26211, 2021.
- [5] Fu Luo, Xi Lin, Zhenkun Wang, Xialiang Tong, Mingxuan Yuan, and Qingfu Zhang. Self-improved learning for scalable neural combinatorial optimization. *arXiv preprint arXiv:2403.19561*, 2024.
- [6] Federico Berto, Chuanbo Hua, Junyoung Park, Laurin Luttman, Yining Ma, Fanchen Bu, Jiarui Wang, Haoran Ye, Minsu Kim, Sanghyeok Choi, Nayeli Gast Zepeda, André Hottung, Jianan Zhou, Jieyi Bi, Yu Hu, Fei Liu, Hyeonah Kim, Jiwoo Son, Haeyeon Kim, Davide Angioni, Wouter Kool, Zhiguang Cao, Jie Zhang, Kijung Shin, Cathy Wu, Sungsoo Ahn, Guojie Song, Changhyun Kwon, Lin Xie, and Jinkyoo Park. RL4CO: an extensive reinforcement learning for combinatorial optimization benchmark. *arXiv preprint arXiv:2306.17100*, 2023.

- [7] Keld Helsgaun. An extension of the lin-kernighan-helsgaun tsp solver for constrained traveling salesman and vehicle routing problems. *Roskilde: Roskilde University*, 12:966–980, 2017.
- [8] Thibaut Vidal. Hybrid genetic search for the cvrp: Open-source implementation and swap\* neighborhood. *Computers & Operations Research*, 140:105643, 2022.
- [9] Paul Shaw. Using constraint programming and local search methods to solve vehicle routing problems. In *International conference on principles and practice of constraint programming*, pages 417–431. Springer, 1998.
- [10] Roberto Baldacci, Aristide Mingozzi, and Roberto Roberti. Recent exact algorithms for solving the vehicle routing problem under capacity and time window constraints. *European Journal of Operational Research*, 218(1):1–6, 2012.
- [11] Oriol Vinyals, Meire Fortunato, and Navdeep Jaitly. Pointer networks. *Advances in neural information processing systems*, 28, 2015.
- [12] Yeong-Dae Kwon, Jinho Choo, Byoungjip Kim, Iljoo Yoon, Youngjune Gwon, and Seungjai Min. POMO: Policy optimization with multiple optima for reinforcement learning. In *Advances in Neural Information Processing Systems*, volume 33, pages 21188–21198, 2020.
- [13] Han Fang, Zhihao Song, Paul Weng, and Yutong Ban. Invt: A generalizable routing problem solver with invariant nested view transformer. In *Forty-first International Conference on Machine Learning*, 2024.
- [14] Simon Geisler, Johanna Sommer, Jan Schuchardt, Aleksandar Bojchevski, and Stephan Günnemann. Generalization of neural combinatorial solvers through the lens of adversarial robustness. In *International Conference on Learning Representations*, 2022.
- [15] Chengrui Gao, Haopu Shang, Ke Xue, Dong Li, and Chao Qian. Towards generalizable neural solvers for vehicle routing problems via ensemble with transferrable local policy. In *Proceedings of the Thirty-First International Joint Conference on Artificial Intelligence*, 2024.
- [16] Darko Drakulic, Sofia Michel, Florian Mai, Arnaud Sors, and Jean-Marc Andreoli. BQ-NCO: Bisimulation quotienting for generalizable neural combinatorial optimization. In *Advances in Neural Information Processing Systems*, 2023.
- [17] Chaoyang Wang, Pengzhi Cheng, Jingze Li, and Weiwei Sun. Leader reward for pomo-based neural combinatorial optimization. *arXiv preprint arXiv:2405.13947*, 2024.
- [18] Yimeng Min, Yiwei Bai, and Carla P Gomes. Unsupervised learning for solving the travelling salesman problem. *Advances in Neural Information Processing Systems*, 2023.
- [19] Yang Li, Jinpei Guo, Runzhong Wang, and Junchi Yan. From distribution learning in training to gradient search in testing for combinatorial optimization. *Advances in Neural Information Processing Systems*, 2023.
- [20] Liang Xin, Wen Song, Zhiguang Cao, and Jie Zhang. Neurolkh: Combining deep learning model with lin-kernighan-helsgaun heuristic for solving the traveling salesman problem. In *Advances in Neural Information Processing Systems*, volume 34, pages 7472–7483, 2021.
- [21] Han Lu, Zenan Li, Runzhong Wang, Qibing Ren, Xijun Li, Mingxuan Yuan, Jia Zeng, Xiaokang Yang, and Junchi Yan. ROCO: A general framework for evaluating robustness of combinatorial optimization solvers on graphs. In *International Conference on Learning Representations*, 2023.
- [22] Sirui Li, Wenbin Ouyang, Max Paulus, and Cathy Wu. Learning to configure separators in branch-and-cut. *Advances in Neural Information Processing Systems*, 36, 2024.
- [23] Taoan Huang, Aaron M Ferber, Arman Zharmagambetov, Yuandong Tian, and Bistra Dilkina. Contrastive predict-and-search for mixed integer linear programs. In Ruslan Salakhutdinov, Zico Kolter, Katherine Heller, Adrian Weller, Nuria Oliver, Jonathan Scarlett, and Felix Berkenkamp, editors, *Proceedings of the 41st International Conference on Machine Learning*, volume 235 of *Proceedings of Machine Learning Research*, pages 19757–19771. PMLR, 21–27 Jul 2024. URL <https://proceedings.mlr.press/v235/huang24f.html>.



- [24] Taoan Huang, Aaron M Ferber, Yuandong Tian, Bistra Dilkina, and Benoit Steiner. Searching large neighborhoods for integer linear programs with contrastive learning. In *International Conference on Machine Learning*, pages 13869–13890. PMLR, 2023.
- [25] Fu Luo, Xi Lin, Fei Liu, Qingfu Zhang, and Zhenkun Wang. Neural combinatorial optimization with heavy decoder: Toward large scale generalization. *Advances in Neural Information Processing Systems*, 36:8845–8864, 2023.
- [26] Zhi Zheng, Changliang Zhou, Tong Xialiang, Mingxuan Yuan, and Zhenkun Wang. Udc: A unified neural divide-and-conquer framework for large-scale combinatorial optimization problems. In *Advances in Neural Information Processing Systems*, 2024.
- [27] Yining Ma, Jingwen Li, Zhiguang Cao, Wen Song, Le Zhang, Zhenghua Chen, and Jing Tang. Learning to iteratively solve routing problems with dual-aspect collaborative transformer. In *Advances in Neural Information Processing Systems*, volume 34, pages 11096–11107, 2021.
- [28] Yining Ma, Zhiguang Cao, and Yeow Meng Chee. Learning to search feasible and infeasible regions of routing problems with flexible neural k-opt. In *Advances in Neural Information Processing Systems*, volume 36, 2023.
- [29] Minjun Kim, Junyoung Park, and Jinkyoo Park. Learning to cross exchange to solve min-max vehicle routing problems. In *The Eleventh International Conference on Learning Representations*, 2023.
- [30] André Hottung and Kevin Tierney. Neural large neighborhood search for routing problems. *Artificial Intelligence*, page 103786, 2022.
- [31] Yining Ma, Jingwen Li, Zhiguang Cao, Wen Song, Hongliang Guo, Yuejiao Gong, and Yeow Meng Chee. Efficient neural neighborhood search for pickup and delivery problems. In *Proceedings of the Thirty-First International Joint Conference on Artificial Intelligence, IJCAI-22*, pages 4776–4784, 7 2022.
- [32] André Hottung, Yeong-Dae Kwon, and Kevin Tierney. Efficient active search for combinatorial optimization problems. In *International Conference on Learning Representations*, 2022.
- [33] Minsu Kim, Jinkyoo Park, and joungho kim. Learning collaborative policies to solve np-hard routing problems. In *Advances in Neural Information Processing Systems*, volume 34, pages 10418–10430, 2021.
- [34] Zhiqing Sun and Yiming Yang. Difusco: Graph-based diffusion solvers for combinatorial optimization. In *Advances in Neural Information Processing Systems*, 2023.
- [35] Felix Chalumeau, Shikha Surana, Clément Bonnet, Nathan Grinsztajn, Arnu Pretorius, Alexandre Laterre, and Thomas D Barrett. Combinatorial optimization with policy adaptation using latent space search. In *Advances in Neural Information Processing Systems*, 2023.
- [36] Minsu Kim, Sanghyeok Choi, Jiwoo Son, Hyeonah Kim, Jinkyoo Park, and Yoshua Bengio. Ant colony sampling with gflownets for combinatorial optimization. *arXiv preprint arXiv:2403.07041*, 2024.
- [37] Ruizhong Qiu, Zhiqing Sun, and Yiming Yang. Dimes: A differentiable meta solver for combinatorial optimization problems. *Advances in Neural Information Processing Systems*, 35: 25531–25546, 2022.
- [38] Alberto Santini, Michael Schneider, Thibaut Vidal, and Daniele Vigo. Decomposition strategies for vehicle routing heuristics. *INFORMS Journal on Computing*, 35(3):543–559, 2023.
- [39] Zefang Zong, Hansen Wang, Jingwei Wang, Meng Zheng, and Yong Li. Rbg: Hierarchically solving large-scale routing problems in logistic systems via reinforcement learning. In *Proceedings of the 28th ACM SIGKDD Conference on Knowledge Discovery and Data Mining*, pages 4648–4658, 2022.
- [40] Haoran Ye, Jiarui Wang, Helan Liang, Zhiguang Cao, Yong Li, and Fanzhang Li. Glop: Learning global partition and local construction for solving large-scale routing problems in real-time. In *Proceedings of the AAAI Conference on Artificial Intelligence*, 2024.

- [41] Qingchun Hou, Jingwei Yang, Yiqiang Su, Xiaoqing Wang, and Yuming Deng. Generalize learned heuristics to solve large-scale vehicle routing problems in real-time. In *The Eleventh International Conference on Learning Representations*, 2023.
- [42] Changliang Zhou, Xi Lin, Zhenkun Wang, and Qingfu Zhang. L2r: Learning to reduce search space for generalizable neural routing solver. *arXiv preprint arXiv:2503.03137*, 2025.
- [43] Shipei Zhou, Yuandong Ding, Chi Zhang, Zhiguang Cao, and Yan Jin. Dualopt: A dual divide-and-optimize algorithm for the large-scale traveling salesman problem. *arXiv preprint arXiv:2501.08565*, 2025.
- [44] Yuxin Pan, Ruohong Liu, Yize Chen, Zhiguang Cao, and Fangzhen Lin. Hierarchical learning-based graph partition for large-scale vehicle routing problems. *arXiv preprint arXiv:2502.08340*, 2025.
- [45] Mouad Morabit, Guy Desaulniers, and Andrea Lodi. Learning to repeatedly solve routing problems. *Networks*, 83(3):503–526, 2024.
- [46] Haoran Ye, Jiarui Wang, Zhiguang Cao, Helan Liang, and Yong Li. DeepACO: Neural-enhanced ant systems for combinatorial optimization. In *Advances in Neural Information Processing Systems*, 2023.
- [47] A Vaswani. Attention is all you need. *Advances in Neural Information Processing Systems*, 2017.
- [48] Petar Veličković, Guillem Cucurull, Arantxa Casanova, Adriana Romero, Pietro Lio, and Yoshua Bengio. Graph attention networks. *arXiv preprint arXiv:1710.10903*, 2017.
- [49] Birger Funke, Tore Grünert, and Stefan Irnich. Local search for vehicle routing and scheduling problems: Review and conceptual integration. *Journal of heuristics*, 11:267–306, 2005.
- [50] Junyoung Chung, Caglar Gulcehre, KyungHyun Cho, and Yoshua Bengio. Empirical evaluation of gated recurrent neural networks on sequence modeling. *arXiv preprint arXiv:1412.3555*, 2014.
- [51] Changliang Zhou, Xi Lin, Zhenkun Wang, Xialiang Tong, Mingxuan Yuan, and Qingfu Zhang. Instance-conditioned adaptation for large-scale generalization of neural combinatorial optimization. *arXiv preprint arXiv:2405.01906*, 2024.
- [52] Marius M Solomon. Algorithms for the vehicle routing and scheduling problems with time window constraints. *Operations research*, 35(2):254–265, 1987.
- [53] Jan Christiaens and Greet Vanden Berghe. Slack induction by string removals for vehicle routing problems. *Transportation Science*, 54(2):417–433, 2020.
- [54] Fei Liu, Tong Xialiang, Mingxuan Yuan, Xi Lin, Fu Luo, Zhenkun Wang, Zhichao Lu, and Qingfu Zhang. Evolution of heuristics: Towards efficient automatic algorithm design using large language model. In *International Conference on Machine Learning*, 2024.
- [55] Marc Goetschalckx and Charlotte Jacobs-Blecha. The vehicle routing problem with backhauls. *European Journal of Operational Research*, 42(1):39–51, 1989.
- [56] Eduardo Uchoa, Diego Pecin, Artur Pessoa, Marcus Poggi, Thibaut Vidal, and Anand Subramanian. New benchmark instances for the capacitated vehicle routing problem. *European Journal of Operational Research*, 257(3):845–858, 2017.
- [57] Florian Arnold, Michel Gendreau, and Kenneth Sörensen. Efficiently solving very large-scale routing problems. *Computers & operations research*, 107:32–42, 2019.

# Learning to Segment for Vehicle Routing Problems (Appendix)

## A Details of First-Segment-Then-Aggregate (FSTA)

### A.1 More discussions on FSTA

#### A.1.1 Visualization of Unstable Edge Patterns

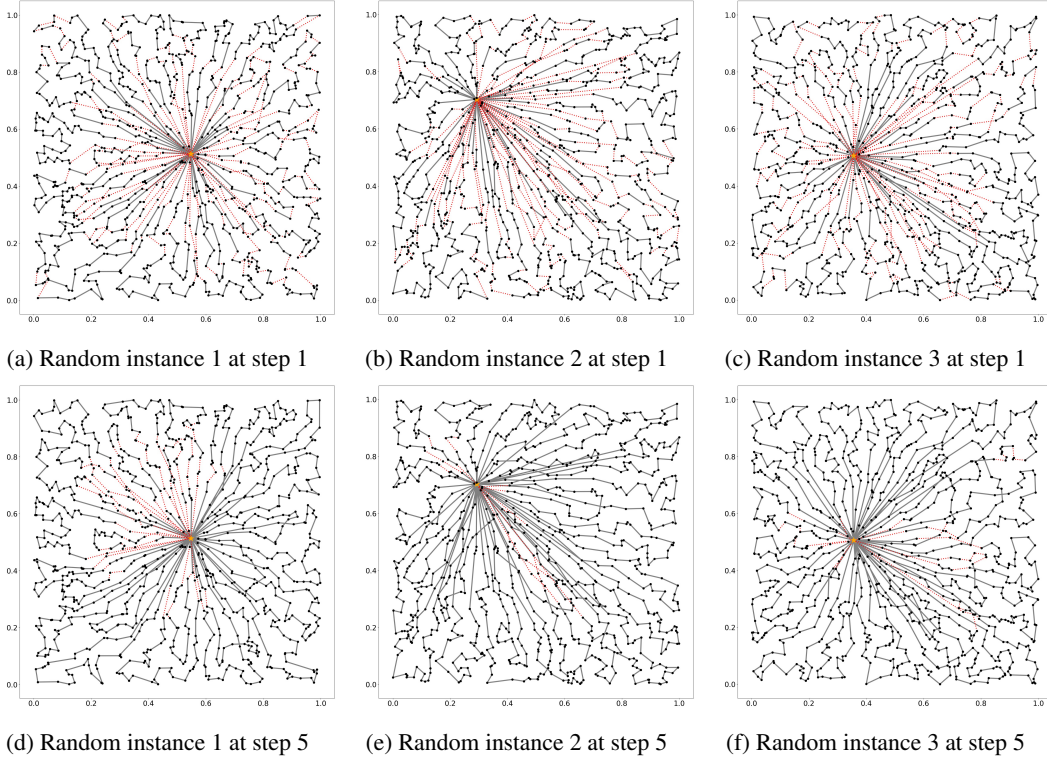


Figure 7: Spatial distribution of unstable edges (dashed red lines) across optimization iterations using LKH-3 solver. Results are presented for three randomly selected CVRP1k instances at iterative search steps 1 and 5. While many edges remain unchanged across iterations, unstable edges predominantly emerge within the interiors of routes. In contrast, edges located at route boundaries exhibit higher stability throughout the iterative optimization process.

In this section, we provide visualization and analysis of unstable edge distribution patterns, which serve as foundational motivation for our L2Seg approach. We examine unstable edges on three randomly selected CVRP1k instances solved iteratively using LKH-3. In these visualizations, red dashed lines represent unstable edges, and yellow stars indicate depot locations.

Our visualization reveals two key observations: (1) The number of unstable edges generally decreases as optimization progresses, with more and more edges remaining unchanged between iterations; (2) Edges at route boundaries exhibit higher stability, while unstable edges predominantly concentrate within route interiors. Despite these discernible spatial patterns, no simple heuristic rule appears sufficient to reliably predict unstable edges, as they can be distributed across the start, middle, and end segments of each tour. This complexity motivates our development of L2Seg, a learning-based method designed to capture these intricate patterns more effectively.

### A.1.2 Visualization of Applying FSTA on One CVRP Instance

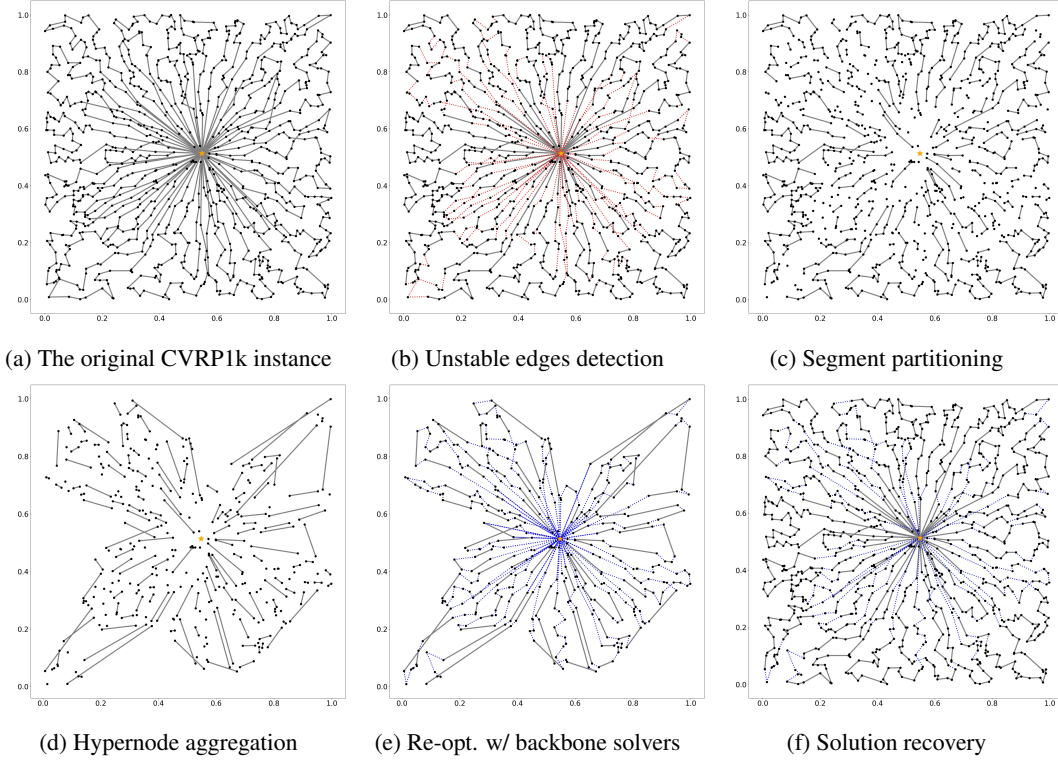


Figure 8: Illustration of our FSTA applied to one CVRP instance. Each FSTA step corresponds to the descriptions in Appendix A.1.4. Red dashed lines: unstable edges; blue dashed lines: re-optimized edges. Note that the subproblem (d) contains substantially fewer nodes than the original instance (a).

To provide a concrete illustration of our FSTA methodology, we present an example of its application to CVRP in Figure 8, which demonstrates the complete FSTA decomposition pipeline (detailed algorithmic specifications are provided in Appendix A.1.4). This example utilizes the lookahead oracle model for unstable edge identification (defined in Appendix A.1.1), employs LKH-3 as the backbone optimization solver, and operates on a representative small-capacity CVRP1k instance to showcase the framework’s efficacy. Red dashed lines indicate detected unstable edges, while blue dashed lines represent re-optimized edges. Note that dual hypernode aggregation substantially reduces the problem size compared to the original instance.

### A.1.3 Assumption Verification

Table 5: Oracle Performance on CVRP2k: Time to Reach L2Seg-SYN-LNS Solution Quality

	Oracle (LNS) + perfect recall & TNR	Oracle (LNS) + 95% recall & 95% TNR	Oracle (LNS) + 90% recall & 90% TNR	Oracle + 70% recall & 70% TNR	Ref (L2Seg-SYN-LNS)
<b>Obj.</b>	56.02	56.01	56.02	56.04	56.08
<b>Time</b>	39s	62s	119s	324s	241s

In Section 3, we hypothesized that effective problem reduction can substantially accelerate re-optimization. We empirically validate this by implementing a look-ahead oracle for unstable edge detection. The oracle performs a 1-step re-optimization using LKH-3 and identifies unstable edges  $E_{\text{unstable}}$  as those differing between the original and re-optimized solutions. FSTA then constructs a reduced problem instance based on these oracle-identified edges, which is subsequently re-optimized using the LKH-3 backbone solver. As this is an oracle-based evaluation, the time required for look-ahead computation is excluded from performance measurements.

Table 5 reports the time required to achieve performance equivalent to our learned model on small-capacity CVRP2k instances. Beyond the perfect oracle scenario, we evaluate imperfect oracle configurations where recall and true negative rates fall below 100%. The perfect oracle demonstrates substantially superior efficiency. Performance remains competitive under moderate imperfection levels; however, achieving recall and TNR as high as 90% without oracle access is highly non-trivial. In more practical scenarios, where recall and TNR drop to 70%, the oracle-based approach is outperformed by our L2Seg-SYN-LNS, highlighting the effectiveness of our learned model.

These results provide evidence that accurate identification of unstable edges, coupled with appropriate FSTA-based problem reduction, enables significantly more efficient re-optimization.

#### A.1.4 Details of FSTA Decomposition Framework

In this section, we present the details of the FSTA decomposition framework. Given a routing problem  $P$  and an initial solution  $\mathcal{R}$ , one iterative step of FSTA yields a potentially improved solution  $\mathcal{R}_+$ . The framework comprises five sequential steps (also illustrated in Algorithm 1 and Figure 2):

1. **Unstable Edges Detection:** We implement effective methods (e.g., our learning-based model L2Seg or random heuristics detailed in Section 5.3) to identify unstable edges  $E_{\text{unstable}}$  and obtain the stable edge set  $E_{\text{stable}} = E \setminus E_{\text{unstable}}$ . This identification challenge is addressed by our L2Seg model, with full details provided in Section 4 and Appendix B.
2. **Segment Partitioning:** After removing unstable edges  $E_{\text{unstable}}$ , each route decomposes into multiple disjoint segments consisting of consecutive nodes connected by stable edges. Formally, we segment each route into  $(x_0, S_{1,j_1}^i, S_{j_1,j_2}^i, \dots, x_0) = (x_0, S_{(1)}^i, S_{(2)}^i, \dots, x_0) \in R^i$ , where  $x_0$  is depot and we simplify the notation by using a single index for segments (note that a segment can consist only one single node).
3. **Hypernode Aggregation:** We aggregate each segment  $S_{j,k}^i$  and represent it with either one hypernode ( $\tilde{S}_{j,k}^i = \{\tilde{x}_{j,k}^i\}$ ) or two hypernodes ( $\tilde{S}_{j,k}^i = \{\tilde{x}_j^i, \tilde{x}_k^i\}$ ) with aggregated attributes. This transformation requires that (our feasibility theorem): (a) the reduced problem remains feasible, and (b) a solution in the aggregated problem can be mapped back to a feasible solution in the original problem. These transformations produce a reduced problem  $\tilde{P}$  with corresponding solution  $\tilde{\mathcal{R}}$ .
4. **Re-optimization with Backbone Solvers:** We invoke a backbone solver to improve solution  $\tilde{\mathcal{R}}$ , yielding an enhanced solution  $\tilde{\mathcal{R}}_+$ . While theoretically any solver could serve as the backbone solver, practical acceleration requires solvers capable of effectively leveraging existing solutions (e.g., LKH-3 [7]).
5. **Solution Recovery:** With the improved solution  $\tilde{\mathcal{R}}_+$  for the reduced problem  $\tilde{P}$ , we recover a corresponding solution  $\mathcal{R}_+$  for the original problem  $P$  by expanding each hypernode back into its original segment of nodes. This step relies on our monotonicity theorem, which guarantees that an improved solution in  $\tilde{P}$  maps to an improved solution in  $P$ .

**Selection of Hypernode Aggregation Strategies.** We analyze the trade-offs between single and dual hypernode aggregation strategies: (1) *Dual hypernode aggregation* enables bidirectional segment traversal, potentially improving re-optimization efficiency by expanding the solution search space. However, this approach requires enforcing inclusion of the connecting edge between hypernodes, adding algorithmic complexity. (2) *Single hypernode aggregation* achieves superior problem size reduction but constrains segment traversal to a fixed direction, thereby restricting the re-optimization search space and potentially limiting performance improvements. Additionally, single hypernode aggregation transforms symmetric routing problems into asymmetric variants, which may compromise the efficiency of existing backbone solvers that are typically optimized for symmetric instances.

**Selection of Backbone Solvers.** Our framework is generic to be applied to most existing VRP heuristics by design. In practice, acceleration within our framework requires solvers that can effectively utilize initial solutions as warm starts. Furthermore, if the dual hypernode aggregation is used, the backbone solver needs to fix certain edges during local search. Our framework is readily compatible with a variety of solvers without modifying their source codes, including LKH-3 [7], decomposition-based solvers like LNS [9], and learning-based methods such as L2D [4]. Incorporating additional solvers such as HGS [8], would involve extending its current code to accept

initial solutions as input, which we leave as future work. Notably, as demonstrated in Section 5, our L2Seg-augmented approach with relatively weaker backbone solvers outperforms HGS in multiple CVRP and VRPTW benchmark scenarios.

**Applicability to Routing Variants.** FSTA is broadly applicable to routing problem variants that support feasible hypernode aggregation and solution recovery, as ensured by the feasibility and monotonicity conditions established in Section 3. In Appendix A.2, we formally prove that many routing variants meet these conditions, demonstrating the versatility of our L2Seg framework. Detailed implementation guidelines for applying hypernode aggregation across different routing variants are provided in Appendix A.1.5.

---

**Algorithm 1:** Iteratively Re-optimize Routing Problems with FSTA

---

**Input:** Routing problem  $P$ , initial solution  $\mathcal{R}$ , time limit  $T_{TL}$ , backbone solver BS, model M to identify unstable edges

**Output:** Improved solution  $\mathcal{R}$

```

1 while time limit  $T_{TL}$  is not reached do
2    $E_{\text{unstable}} \leftarrow M(P, \mathcal{R})$ ; // Unstable Edges Detection
3    $\{S_{j,k}^i\} \leftarrow \text{GetSegments}(P, \mathcal{R}, E_{\text{unstable}})$ ; // Segment Partitioning
4   Obtain  $\{\tilde{S}_{j,k}^i\}$  and reduced problem  $\tilde{P}$  with solution  $\tilde{\mathcal{R}}$ ; // Hypernode Aggregation
5    $\tilde{\mathcal{R}}_+ \leftarrow \text{BS}(\tilde{P}, \tilde{\mathcal{R}})$ ; // Re-optimization with Backbone Solver
6    $\mathcal{R}_+ \leftarrow \text{RecoverSolution}(P, \tilde{P}, \tilde{\mathcal{R}}_+)$ ; // Solution Recovery
7    $\mathcal{R} \leftarrow \mathcal{R}_+$ ; // Update current solution
8 end while
9 return  $\mathcal{R}$ 

```

---

### A.1.5 Applying FSTA on Various VRPs

In this section, we present the implementation details of FSTA across diverse routing variants, including the Capacitated Vehicle Routing Problem (CVRP), Vehicle Routing Problem with Time Windows (VRPTW), Vehicle Routing Problem with Backhauls (VRPB), Single-Commodity Vehicle Routing Problem with Pickup and Delivery (1-VRPPD), and Risk-Constrained Cash-in-Transit Vehicle Routing Problem (RCTVRP). Without loss of generality, we denote a segment to be aggregated as  $S_{j,k} = (x_j \rightarrow \dots \rightarrow x_k)$ , and its corresponding hypernode representation as either  $\tilde{S}_{j,k} = \{\tilde{x}\}$  (single hypernode) or  $\tilde{S}_{j,k} = \{\tilde{x}_j, \tilde{x}_k\}$  (dual hypernodes). The implementation specifications are summarized in Table 6.

**CVRP.** We provide the formal definition of CVRP in Section 3. Each node in CVRP is characterized by location and demand attributes. For CVRP, we employ dual hypernode aggregation where location attributes are preserved as  $\tilde{x}_j = x_j$  and  $\tilde{x}_k = x_k$ , while demand is equally distributed between hypernodes as  $\tilde{d}_j = \tilde{d}_k = \frac{1}{2}(d_j + \dots + d_k)$ . We force the solver to include the edge connecting  $\tilde{x}_j$  and  $\tilde{x}_k$  in the solution.

**VRPTW.** We provide the formal definition of VRPTW in Section 3. In addition to location and demand attributes, VRPTW instances are characterized by time windows  $[t^l, t^r]$  and service time  $s$  for each node. For VRPTW, we employ adaptive strategies for hypernode aggregation based on temporal feasibility. We first compute the aggregated time windows  $\bar{t}_j^l, \bar{t}_j^r$  and aggregated service time  $\bar{s}_j$  using the following recursive formulation:

$$\begin{aligned}
\bar{t}_m^l &= \begin{cases} t_k^l & \text{if } m = k \\ \max\{t_m^l, \bar{t}_{m+1}^l - (s_m + \text{dist}(x_m, x_{m+1}))\} & \text{if } j \leq m \leq k-1, \end{cases} \\
\bar{t}_m^r &= \begin{cases} t_k^r & \text{if } m = k \\ \min\{t_m^r, \bar{t}_{m+1}^r - (s_m + \text{dist}(x_m, x_{m+1}))\} & \text{if } j \leq m \leq k-1, \end{cases} \\
\bar{s}_m &= \begin{cases} s_k & \text{if } m = k \\ \bar{s}_{m+1} + s_m + \text{dist}(x_m, x_{m+1}) & \text{if } j \leq m \leq k-1, \end{cases}
\end{aligned} \tag{3}$$

where  $[t_m^l, t_m^r]$  denotes the time window for node  $x_m$ ,  $s_m$  represents the service time at node  $x_m$ , and  $\text{dist}(x_m, x_{m+1})$  is the travel time from node  $x_m$  to node  $x_{m+1}$ .

If  $\bar{t}_j^l \leq \bar{t}_j^r$  (feasible time window), we employ single hypernode aggregation with:  $\text{dist}(x_i, \tilde{x}) = \text{dist}(x_i, x_j)$ ,  $\text{dist}(\tilde{x}, x_i) = \text{dist}(x_k, x_i)$ ,  $\tilde{d} = d_j + \dots + d_k$ ,  $\tilde{t}^l = \bar{t}_j^l$ ,  $\tilde{t}^r = \bar{t}_j^r$ , and  $\tilde{s} = \bar{s}_j$ .

If  $\bar{t}_j^l > \bar{t}_j^r$  (temporal infeasible time window), we employ dual hypernode aggregation with:  $\tilde{x}_j = x_j$ ,  $\tilde{x}_k = x_k$ ,  $\tilde{d}_j = \tilde{d}_k = \frac{1}{2}(d_j + \dots + d_k)$ , time windows  $\tilde{t}_j^l = 0$ ,  $\tilde{t}_j^r = \bar{t}_j^r$ ,  $\tilde{t}_k^l = \bar{t}_j^l$ ,  $\tilde{t}_k^r = \infty$ , and service times  $\tilde{s}_j = 0$ ,  $\tilde{s}_k = \bar{s}_j$ . We additionally set  $\text{dist}(\tilde{x}_j, \tilde{x}_k) = 0$  and enforce inclusion of the edge connecting  $\tilde{x}_j$  and  $\tilde{x}_k$  in the solution.

**VRPB.** Compared to the CVRP, The VRPB [55] involves serving two types of customers: linehaul customers requiring deliveries from the depot and backhaul customers providing goods to be collected and returned to the depot. The primary constraint is that all linehaul customers must be visited before any backhaul customers on the same route, while ensuring vehicle capacity is never exceeded during either the delivery or pickup phases. We use  $b_i \in \{0, 1\}$  to indicate whether node  $i$  is a backhaul customer. For VRPB, we require the edge connecting to a linehaul customer and a backhaul customer included in the  $E_{\text{unstable}}$ . We employ single hypernode aggregation that  $\text{dist}(x_i, \tilde{x}) = \text{dist}(x_i, x_j)$ ,  $\text{dist}(\tilde{x}, x_i) = \text{dist}(x_k, x_i)$ ,  $\tilde{d} = d_j + \dots + d_k$ , and  $\tilde{b} = b_j$  (we require customer being the same type within each segment that  $b_j = \dots = b_k$ ).

Table 6: Implementation specifications of FSTA hypernode aggregation for CVRP, VRPTW, and VRPB variants. Refer to Equation 3 for the definitions of  $\bar{s}_j$ ,  $\bar{t}_j^l$  and  $\bar{t}_j^r$ .

CVRP				
Type	Condition	Attribute	Aggregation	Additional Constraints / Settings
Two Hypernodes	Always	Location/Distance	$\tilde{x}_j = x_j$	Include edge $\tilde{x}_j \rightarrow \tilde{x}_k$ in the solution
		Demand	$\tilde{x}_k = x_k$ $\tilde{d}_j = \tilde{d}_k = \frac{1}{2}(d_j + \dots + d_k)$	
VRPTW				
Type	Condition	Attribute	Aggregation	Additional Constraints / Settings
One Hypernode	$\bar{t}_j^l \leq \bar{t}_j^r$	Location/Distance	$\text{dist}(x_i, \tilde{x}) = \text{dist}(x_i, x_j)$ , $\text{dist}(\tilde{x}, x_i) = \text{dist}(x_k, x_i)$	None
		Demand	$\tilde{d} = d_j + \dots + d_k$	
		Service Time	$\tilde{s} = \bar{s}_j$	
		Time Windows	$\bar{t}^l = \bar{t}_j^l, \bar{t}^r = \bar{t}_j^r$	
Two Hypernodes	$\bar{t}_j^l > \bar{t}_j^r$	Location/Distance	$\tilde{x}_j = x_j, \tilde{x}_k = x_k$	Include edge $\tilde{x}_j \rightarrow \tilde{x}_k$ in solution; set $\text{dist}(\tilde{x}_j, \tilde{x}_k) = 0$
		Demand	$\tilde{d}_j = \tilde{d}_k = \frac{1}{2}(d_j + \dots + d_k)$	
		Service Time	$\tilde{s}_j = 0, \tilde{s}_k = \bar{s}_j$	
		Time Windows	$\bar{t}_j^l = 0, \bar{t}_j^r = \bar{t}_j^r, \bar{t}_k^l = \bar{t}_j^l, \bar{t}_k^r = \infty$	
VRPB				
Type	Condition	Attribute	Aggregation	Additional Constraints / Settings
One Hypernode	Always	Location/Distance	$\text{dist}(x_i, \tilde{x}) = \text{dist}(x_i, x_j)$ , $\text{dist}(\tilde{x}, x_i) = \text{dist}(x_k, x_i)$	Require $b_j = \dots = b_k$ (same customer type) during Unstable Edges Detection Stage
		Demand	$\tilde{d} = d_j + \dots + d_k$	
		Is backhaul	$\tilde{b} = b_j$	

## A.2 Proof of FSTA

**Theorem. (Feasibility)** If the aggregated solution  $\tilde{\mathcal{R}}_+$  is a feasible solution to the aggregated problem, then  $\mathcal{R}_+$  is a feasible solution to the original, non-aggregated problem. *(Monotonicity)* Let  $\tilde{\mathcal{R}}_+^1$  and  $\tilde{\mathcal{R}}_+^2$  be two feasible solutions to the aggregated problem, with  $f(\tilde{\mathcal{R}}_+^1) \leq f(\tilde{\mathcal{R}}_+^2)$ , where  $f(\cdot)$  denotes the objective function (total travel cost). Then, for the associated solution in the original space, we also have  $f(\mathcal{R}_+^1) \leq f(\mathcal{R}_+^2)$ .

**Proof Structure and Notation.** Without loss of generality, we consider a single-route solution containing one segment  $S_{j,k} = (x_j \rightarrow \dots \rightarrow x_k)$  with more than one node, i.e., the solution  $\mathcal{R}$  contains route  $R = (x_0 \rightarrow x_1 \rightarrow \dots \rightarrow S_{j,k} \rightarrow x_{k+1} \rightarrow \dots \rightarrow x_0)$ . We define the aggregated problem with node set  $\tilde{V} = \{x_0\} \cup \{x_p\}_{p < j} \cup \{\tilde{S}_{j,k}\}$ , where nodes outside the segment retain their original representation, ensuring their feasibility by construction. Since we enforce the inclusion of the edge connecting  $\tilde{x}_j$  and  $\tilde{x}_k$  in dual hypernode aggregation within solution  $\tilde{\mathcal{R}}_+$ , the segment



$\tilde{S}_{j,k}$  must be incorporated into some route  $\tilde{R}_+^* \in \tilde{\mathcal{R}}_+$  for both hypernode aggregation strategies. We denote the improved route containing this segment after mapping back to the original problem as  $R_+^*$ .

We present the segment aggregation strategies for different routing variants below, followed by proofs of feasibility and monotonicity for the aggregation scheme. Note that the following analysis naturally extends to multi-route solutions with multiple segments per route.

### A.2.1 CVRP

**Aggregation Strategy (Two Hypernodes).** The detailed implementation of FSTA on CVRP can be found in Appendix A.1.5 and Table 6. Notice that one single hypernode aggregation is also applicable for CVRP, and  $\tilde{d}_j, \tilde{d}_k$  could take other values as long as  $\tilde{d}_j + \tilde{d}_k = d_j + \dots + d_k$ .

**Feasibility Proof [Capacity Constraint].** Notice that since  $\tilde{d}_j + \tilde{d}_k = d_j + \dots + d_k$ , we have:

$$\begin{aligned} \sum_{x_i \in \tilde{R}_+^*} d_i &= \sum_{x_i \in \tilde{R}_+^* \setminus \tilde{S}_{j,k}} d_i + \tilde{d}_j + \tilde{d}_k \\ &= \sum_{x_i \in R_+^* \setminus S_{j,k}} d_i + d_j + \dots + d_k = \sum_{x_i \in R_+^*} d_i \end{aligned} \quad (4)$$

Thus, we have:

$$\sum_{x_i \in \tilde{R}_+^*} d_i \leq C \Rightarrow \sum_{x_i \in R_+^*} d_i \leq C \quad (5)$$

Then, we have a feasible  $\tilde{\mathcal{R}}_+ \Rightarrow$  a feasible  $\mathcal{R}_+$ .

□

**Monotonicity Proof.** Notice that

$$\begin{aligned} f(\tilde{\mathcal{R}}_+) &= f(\tilde{\mathcal{R}}_+ \setminus \{\tilde{R}_+^*\}) + f(\{\tilde{R}_+^*\}) = f(\mathcal{R}_+ \setminus \{R_+^*\}) + f(\{\tilde{R}_+^*\}) \\ &= f(\mathcal{R}_+ \setminus \{R_+^*\}) + f(\{R_+^*\}) - \sum_{j \leq q < k} \text{dist}(x_q, x_{q+1}) + \text{dist}(\tilde{x}_j, \tilde{x}_k) \\ &= f(\mathcal{R}_+) + \text{Const}|_{S_{j,k}} \end{aligned} \quad (6)$$

where  $\text{Const}|_{S_{j,k}}$  is a constant once the segment  $S_{j,k}$  is decided. Therefore, we have:

$$f(\tilde{\mathcal{R}}_+^1) \leq f(\tilde{\mathcal{R}}_+^2) \Rightarrow f(\mathcal{R}_+^1) + \text{Const}|_{S_{j,k}} \leq f(\mathcal{R}_+^2) + \text{Const}|_{S_{j,k}} \Rightarrow f(\mathcal{R}_+^1) \leq f(\mathcal{R}_+^2) \quad (7)$$

□

We note that the feasibility proof for capacity constraint and the monotonicity proof could be easily extended to the single hypernodes aggregation.

### A.2.2 VRPTW

**Aggregation Strategy (Mixed Strategies).** The detailed implementation of FSTA on VRPTW can be found in Appendix A.1.5 and Table 6. We denote  $s_m^* = s_m + \text{dist}(x_m, x_{m+1})$  for  $j \leq m < k$  and  $s_k^* = s_k$ . We further set the service time by  $\tilde{s}_m = \sum_{m \leq q \leq k} s_q^*$ , and we repeat the temporal time

window  $[\bar{t}_j^l, \bar{t}_j^r]$  (which could be infeasible) defined by the following recursive relationship:

$$\begin{aligned} \bar{t}_m^l &= \begin{cases} t_k^l & m = k \\ \max\{t_m^l, \bar{t}_{m+1}^l - s_m^*\} & j \leq m \leq k-1, \end{cases} \\ \bar{t}_m^r &= \begin{cases} t_k^r & m = k \\ \min\{t_m^r, \bar{t}_{m+1}^r - s_m^*\} & j \leq m \leq k-1, \end{cases} \end{aligned} \quad (8)$$

where  $[t_m^l, t_m^r]$  is the time window for a node  $x_m$ ,  $s_m$  is the service time at node  $x_m$  and  $\text{dist}(x_m, x_{m+1})$  is the time to travel from node  $x_m$  to node  $x_{m+1}$ .

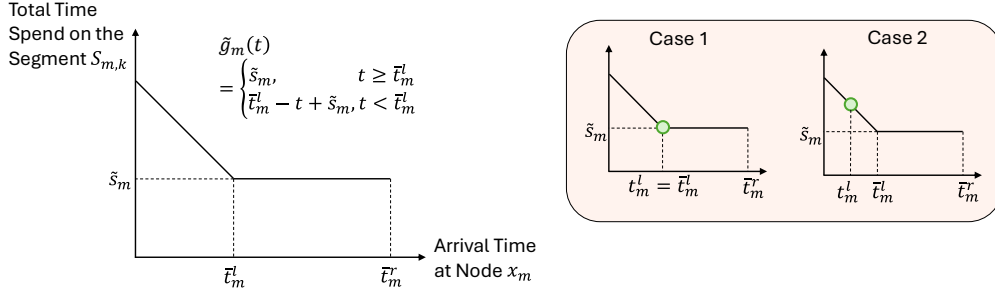


Figure 9: This illustration demonstrates the temporal dynamics of the aggregated segment. The left panel shows the time function characterized by a piecewise linear structure: initially decreasing with slope -1, then transitioning to a constant value corresponding to the aggregated left time window boundary. The right panel presents two distinct scenarios that characterize the relationship between the aggregated left time window ( $\bar{t}_m^l$ ) and the individual non-aggregated left time windows ( $t_m^l$ ).

**Feasibility Proof [Time Window Constraint].** We first prove for the condition that the temporal time window  $[\bar{t}_j^l, \bar{t}_j^r]$  is feasible ( $\bar{t}_j^l < \bar{t}_j^r$ ) and single hypernode aggregation is applied. Then, we extend to the infeasible temporal time window condition where dual hypernode aggregation is applied.

**Condition of Feasible Temporal Time Windows (One Hypernode).** We present an inductive proof based on the *segment length*. Given a feasible solution  $\tilde{\mathcal{R}}_+$  for the aggregated problem, we show the following two conditions of the corresponding non-aggregated solution  $\mathcal{R}_+$  to satisfy the time window constraint:

- *Condition (1):* We visit each node  $x_m$  before the end of its time window  $t_m^r$ .
- *Condition (2):* The total time we spent visiting the entire segment is the same in both aggregated and non-aggregated representations.

*Proof of Condition (1):*

- *Base case (segment length = 1).* Suppose the segment  $S_{k,k} = (x_k)$  contains a single node  $x_k$ . Then the aggregated problem is identical to the non-aggregated problem by construction, so condition (1) is trivially satisfied.
- *Inductive Step (segment length =  $(k - m) + 1 > 1$ ).* textit the aggregation of the segment  $S_{m+1,k} = (x_{m+1} \rightarrow \dots \rightarrow x_k)$  into  $\tilde{S}_{m+1,k} = \{\tilde{x}_{m+1,k}\}$  satisfies condition (1). We want to show that the aggregation of the segment  $S_{m,k} = (x_m \rightarrow \dots \rightarrow x_k)$  into  $\tilde{S}_{m,k} = \{\tilde{x}_{m,k}\}$  also satisfies condition (1).

Since  $\tilde{\mathcal{R}}_+$  is a feasible solution for the aggregated problem, we will visit the hypernode  $\tilde{x}_{m,k}$  before the end of its time window  $\bar{t}_m^r = \min\{t_m^r, \bar{t}_{m+1}^r - s_m^*\}$ . Corresponding, in the associated non-aggregated solution, we visit the node  $x_m$  before its time limit  $t_m^r$ , hence satisfying condition (1) for the node  $x_m$ . Furthermore, in the associated non-aggregated solution, we visit the next node  $x_{m+1}$  before time  $\bar{t}_m^r + s_m^* \leq \bar{t}_{m+1}^r$ . Based on the inductive hypothesis, condition (1) holds for the rest of the segment  $(x_{m+1} \rightarrow \dots \rightarrow x_k)$  if we arrive at node  $x_{m+1}$  before its end time. Hence, condition (1) holds for the whole segment  $S_{m,k} = (x_m \rightarrow x_{m+1} \rightarrow \dots \rightarrow x_k)$ .

*Proof of Condition (2):* For all  $m$ , suppose we arrive at the hypernode  $\tilde{x}_{m,k}$  at time  $t \leq \bar{t}_m^r$  in the aggregated solution. By definition, the total time spent on the aggregated segment (sum of the waiting time, service time, and the travel time) can be written as the following linear function with  $-1$  slope as shown in the first figure in Figure 9.

$$\tilde{g}_m(t) = \begin{cases} \tilde{s}_m & t \geq \bar{t}_m^l \\ \bar{t}_m^l - t + \tilde{s}_m & t < \bar{t}_m^l \end{cases} \quad (9)$$

Note: the first condition  $t \geq \bar{t}_m$  means we do not need to wait at any node in the segment  $S_{m,k}$ , and the second condition means we need to wait at some node in the segment  $S_{m,k}$ .

It suffices to show that the total time spent on the non-aggregated segment also follows the same function. Again, we prove this by induction.

- *Base case (segment length = 1).* Suppose the segment  $S_{k,k} = (x_k)$  contains a single node  $x_k$ . Then the aggregated problem is identical to the non-aggregated problem by construction, so the total time spent on the non-aggregated segment is exactly Eq. 9 with  $m = k$ .
- *Inductive Step (segment length =  $(k - m) + 1 > 1$ ).* Again, suppose the total time spent on the segment  $S_{m+1,k} = (x_{m+1} \rightarrow \dots \rightarrow x_k)$  into  $\tilde{S}_{m+1,k} = \{\tilde{x}_{m+1,k}\}$  satisfies the function

$$g_{m+1}(t) = \tilde{g}_{m+1}(t) = \begin{cases} \tilde{s}_{m+1} & t \geq \bar{t}_{m+1}^l \\ \bar{t}_{m+1}^l - t + \tilde{s}_{m+1} & t < \bar{t}_{m+1}^l \end{cases} \quad (10)$$

We now show the total time function  $g_m(t)$  for the segment  $S_{m,k} = (x_m \rightarrow \dots \rightarrow x_k)$  also equals  $\tilde{g}_m(t)$ .

By definition of the non-aggregated segment, depending on whether we need to wait at the first node  $x_m$ , we have:

$$g_m(t) = \begin{cases} s_m^* + g_{m+1}(t + s_m^*) & t \geq t_m^l \\ t_m^l - t + s_m^* + g_{m+1}(t_m^l + s_m^*) & t < t_m^l. \end{cases} \quad (11)$$

Note: the first condition  $t \geq t_m^l$  means we do not need to wait at the first node  $x_m$ , and the second condition  $t < t_m^l$  means we need to wait at the first node  $x_m$ .

We split the discussion into the following two cases, based on whether we need to wait at any node along the segment  $S_{m+1,k}$ , if we leave node  $x_m$  at  $t_m^l$ :

1.  $t_m^l + s_m^* \geq \bar{t}_{m+1}^l$ . In this case,  $t_m^l \geq \bar{t}_{m+1}^l - s_m^*$ , and hence  $\bar{t}_m^l = \max\{t_m^l, \bar{t}_{m+1}^l - s_m^*\} = t_m^l$  as shown in case 1 of Figure 9. Hence, we have

$$g_m(t) = \begin{cases} s_m^* + g_{m+1}(t + s_m^*) & t \geq \bar{t}_m^l \\ t_m^l - t + s_m^* + g_{m+1}(t_m^l + s_m^*) & t < \bar{t}_m^l. \end{cases} \quad (12)$$

By inductive hypothesis, we have

$$g_{m+1}(t + s_m^*) = \tilde{s}_{m+1}, \quad t \geq t_m^l = \bar{t}_m^l,$$

as in this case  $t + s_m^* \geq t_m^l + s_m^* \geq \bar{t}_{m+1}^l$ .

Hence, we have

$$\begin{aligned} g_m(t) &= \begin{cases} s_m^* + \tilde{s}_{m+1} & t \geq \bar{t}_m^l \\ t_m^l - t + s_m^* + \tilde{s}_{m+1} & t < \bar{t}_m^l. \end{cases} \\ &= \begin{cases} \tilde{s}_m & t \geq \bar{t}_m^l \\ t_m^l - t + \tilde{s}_m & t < \bar{t}_m^l \end{cases} = \tilde{g}_m(t). \end{aligned} \quad (13)$$

where we apply the definition of  $\tilde{s}_m = s_m^* + \tilde{s}_{m+1}$ .

2.  $t_m^l + s_m^* < \bar{t}_{m+1}^l$ . In this case,  $\bar{t}_{m+1}^l - s_m^* > t_m^l$ , and hence  $\bar{t}_m^l = \max\{t_m^l, \bar{t}_{m+1}^l - s_m^*\} = \bar{t}_{m+1}^l - s_m^*$  as shown in case 2 of Figure 9.

By inductive hypothesis, we have

$$\begin{aligned} g_{m+1}(t_m^l + s_m^*) &= \bar{t}_{m+1}^l - (t_m^l + s_m^*) + \tilde{s}_{m+1} \\ &= \bar{t}_m^l - t_m^l + \tilde{s}_{m+1} \end{aligned} \quad (14)$$

We also have, for all  $t \geq t_m^l$ ,

$$\begin{aligned} &g_{m+1}(t + s_m^*) \\ &= \begin{cases} \tilde{s}_{m+1}, & t + s_m^* \geq \bar{t}_{m+1}^l \\ \bar{t}_{m+1}^l - (t + s_m^*) + \tilde{s}_{m+1}, & t + s_m^* < \bar{t}_{m+1}^l \end{cases} \\ &= \begin{cases} \tilde{s}_{m+1}, & t \geq \bar{t}_m^l \\ \bar{t}_m^l - t + \tilde{s}_{m+1}, & t_m^l \leq t < \bar{t}_m^l \end{cases} \end{aligned} \quad (15)$$

As a result, we have

$$\begin{aligned}
g_m(t) &= \begin{cases} s_m^* + \tilde{s}_{m+1} & t \geq \bar{t}_m^l \\ s_m^* + \bar{t}_m - t + \tilde{s}_{m+1} & \bar{t}_m^l \leq t < \bar{t}_m^l \\ \bar{t}_m^l - t + s_m^* + \bar{t}_m^l - \bar{t}_m^l + \tilde{s}_{m+1} & t < \bar{t}_m^l, \end{cases} \\
&= \begin{cases} \tilde{s}_m & t \geq \bar{t}_m^l \\ \bar{t}_m - t + \tilde{s}_m & \bar{t}_m^l \leq t < \bar{t}_m^l \\ \bar{t}_m^l - t + \tilde{s}_m & t < \bar{t}_m^l, \end{cases} \\
&= \begin{cases} \tilde{s}_m & t \geq \bar{t}_m^l \\ \bar{t}_m^l - t + \tilde{s}_m & t < \bar{t}_m^l \end{cases} = \tilde{g}_m(t).
\end{aligned} \tag{16}$$

**Condition of Infeasible Temporal Time Windows (Two Hypernodes).** In our time window aggregation,  $\bar{t}_j^l$  is responsible for the time expenditure and  $\bar{t}_j^r$  is responsible for feasibility. In this case, we have  $\bar{t}_j^l > \bar{t}_j^r$ , which indicates that to maintain feasibility along the segment, one must arrive at the segment before the aggregated start time  $\bar{t}_j^l$ , and since one arrives earlier, one must wait at some node within the segment. Since  $\bar{t}_j^l > \bar{t}_j^r$  is not permitted according to the definition of VRPTW, we then utilize one additional hypernode to increase the representational capacity such that the first hypernode handles the feasibility component ( $\bar{t}_j^r$ ), and the second hypernode handles the travel time component ( $\bar{t}_j^l$ ). Specifically,  $\bar{t}_j^l = 0$ ,  $\bar{t}_j^r = \bar{t}_j^r$ ,  $\bar{t}_k^l = \bar{t}_j^l$ ,  $\bar{t}_k^r = \infty$  and  $\tilde{s}_j = 0$ ,  $\tilde{s}_k = \bar{s}_j$  with the additional constraint that  $\text{dist}(\tilde{x}_j, \tilde{x}_k) = 0$ .

For time window feasibility (Condition (1)), since  $\bar{t}_j^r = \bar{t}_j^r$ , the vehicle must serve the segment before  $\bar{t}_j^r$ , ensuring the feasibility of serving each customer in the non-aggregated problem. For travel time equivalence (Condition (2)), the time expended before reaching the second node is  $\tilde{s}_j + \text{dist}(\tilde{x}_j, \tilde{x}_k) = 0$ . Namely, after the vehicle arrives at the segment at time  $t$ , the travel time is entirely determined by  $\bar{t}_k^l = \bar{t}_j^l$  and  $\tilde{s}_k = \bar{s}_j$ , whereby in the feasible temporal time window situation, the travel time equivalence is demonstrated.

We complete the time window constraint feasibility proof for VRPTW for both aggregation strategies across all conditions.

□

**Monotonicity Proof.** For the dual hypernode aggregation, please refer to the *Monotonicity Proof* in A.2.1. For the single hypernode aggregation, notice that

$$\begin{aligned}
f(\tilde{\mathcal{R}}_+) &= f(\tilde{\mathcal{R}}_+ \setminus \{\tilde{R}_+^*\}) + f(\{\tilde{R}_+^*\}) = f(\mathcal{R}_+ \setminus \{R_+^*\}) + f(\{\tilde{R}_+^*\}) \\
&= f(\mathcal{R}_+ \setminus \{R_+^*\}) + f(\{R_+^*\}) - \sum_{j \leq q < k} \text{dist}(x_q, x_{q+1}) \\
&= f(\mathcal{R}_+) + \text{Const}|_{S_{j,k}}
\end{aligned} \tag{17}$$

where  $\text{Const}|_{S_{j,k}}$  is a constant once the segment  $S_{j,k}$  is decided. Therefore, we have:

$$f(\tilde{\mathcal{R}}_+^1) \leq f(\tilde{\mathcal{R}}_+^2) \Rightarrow f(\mathcal{R}_+^1) + \text{Const}|_{S_{j,k}} \leq f(\mathcal{R}_+^2) + \text{Const}|_{S_{j,k}} \Rightarrow f(\mathcal{R}_+^1) \leq f(\mathcal{R}_+^2) \tag{18}$$

□

### A.2.3 VRPB

**Aggregation Strategy (One Hypernode).** The detailed implementation of FSTA on VRPB can be found in Appendix A.1.5 and Table 6.

**Feasibility Proof [Backhaul Constraint].** Without loss of generality, we assume all nodes within the segment  $S_{j,k}$  are backhaul customers ( $b_j = \dots = b_k = 1$ ). Notice that since  $\tilde{d} = d_j + \dots + d_k$ , for the backhaul stage, we have:

$$\begin{aligned}
\sum_{x_i \in \tilde{R}_+^* \text{ and } b_i=1} d_i &= \sum_{x_i \in \tilde{R}_+^* \setminus \tilde{S}_{j,k} \text{ and } b_i=1} d_i + \tilde{d} \\
&= \sum_{x_i \in R_+^* \setminus S_{j,k} \text{ and } b_i=1} d_i + d_j + \dots + d_k = \sum_{x_i \in R_+^* \text{ and } b_i=1} d_i
\end{aligned} \tag{19}$$

For the linehaul stage, we have:

$$\sum_{x_i \in \tilde{R}_+^* \text{ and } b_i=0} d_i = \sum_{x_i \in R_+^* \text{ and } b_i=0} d_i \quad (20)$$

Thus, we have:

$$\begin{aligned} \sum_{x_i \in \tilde{R}_+^* \text{ and } b_i=0} d_i \leq C &\Rightarrow \sum_{x_i \in R_+^* \text{ and } b_i=0} d_i \leq C \\ \sum_{x_i \in \tilde{R}_+^* \text{ and } b_i=1} d_i \leq C &\Rightarrow \sum_{x_i \in R_+^* \text{ and } b_i=1} d_i \leq C \end{aligned} \quad (21)$$

Then, we have a feasible  $\tilde{\mathcal{R}}_+ \Rightarrow$  a feasible  $\mathcal{R}_+$ .

□

**Monotonicity Proof.** Please refer to the monotonicity proof of VRPTW in Appendix A.2.2.

## B L2Seg Details

### B.1 Input Feature Design Details

Previous works [2, 4, 12] typically utilize only basic input features for routing problems (xy-coordinates and normalized demands for node features, and edge cost for edge features). While neural networks can potentially learn complex patterns from these basic features, tailored feature engineering may lead to enhanced model performance. As illustrated in Appendix A.1, we observe that detecting unstable edges may depend on better capturing local dependencies. We therefore design enhanced node and edge features for our learning task, as shown in Table 7. We also include time windows and service time as node features for VRPTWs.

Table 7: Description of enhanced input features for nodes and edges.

Type	Description	Dimension
<b>Nodes</b>	The xy coordinates	2
	The normalized demand	1
	The centroid of the subtour for each node	2
	The coordinates of the two nodes connecting to each node	4
	The travel cost of the two edges connecting to each node	2
	The relative xy coordinates	2
	The angles w.r.t. the depot	1
	The weighted angles w.r.t. the depot by the distances	1
	The distances of the closest 3 neighbor for each node	3
	The percentage of the K nearest nodes that are within the same subtour. K=5, 15, 40	3
	The percentage of the K% nearest nodes that are within the same subtour. K=5, 15, 40	3
	The travel cost	1
<b>Edges</b>	Whether each edge is within the current solution	1
	The travel cost rank of each edge w.r.t. the corresponding end points	1

### B.2 Masking Details

In general, any set of unstable edges could lead to a feasible FSTA problem reduction. However, employing logic-based local search algorithms to select unstable edges can produce more reasonable action space reduction and improved performance. Thus, we design the deletion and insertion stages of L2Seg to emulate a general local search operation.

**For the deletion stage**, given the current node  $x$ , we mask out nodes that are: (1) not connected to  $x$ ; or (2) part of an edge that has already been deleted during the current deletion stage. Note that the model may select the special ending node  $x_{\text{end}}$  to terminate the decoding sequence.

**For the insertion stage**, given the current node  $x$ , we mask out nodes that are: (1) already connected to  $x$ ; (2) endpoints of two newly inserted edges; or (3) the special ending node  $x_{\text{end}}$ .

### B.3 Training Data Collection Details

In this section, we present pseudocode that demonstrate the process of generating training labels for both NAR and AR models in Algorithm 2. As a complement to the methodology described in Section 4, we derive our training data from  $N_{\mathcal{P}}$  distinct problem instances and extract labels from the first  $T_{IS}$  iterative improvement steps. For the AR labels, which emulate feasible local search operations, each label (representing a sequence of nodes) is associated with a quantifiable improvement in solution quality. We retain only those labels that yield improvements exceeding the threshold  $\eta_{\text{improv}}$ , and we employ stochastic sampling by accepting labels with probability  $\alpha_{AC}$ . This selective approach ensures both high-quality training signals and sufficient diversity across problem instances and optimization trajectories within the same training budget.

---

#### Algorithm 2: Training Data Generation

---

**Input:** Solution distribution  $\mathcal{P}$ , number of instances  $N_{\mathcal{P}}$ , backbone solver  $BS$ , number of iterative steps  $T_{IS}$ , improvement threshold  $\eta_{\text{improv}}$ , sample coefficient  $\alpha_{AC}$

**Output:** Label sets  $\mathcal{Y}_{\text{NAR}}, \mathcal{Y}_{\text{AR}}$

```

1  $\mathcal{Y}_{\text{NAR}} \leftarrow \emptyset, \mathcal{Y}_{\text{AR}} \leftarrow \emptyset$  for  $i \leftarrow 1$  to  $N_{\mathcal{P}}$  do
2   Sample  $P \sim \mathcal{P}$  and obtain an initial solution  $\mathcal{R}$ 
3   for  $t \leftarrow 1$  to  $T_{IS}$  do
4      $\mathcal{R}_+ \leftarrow BS(P, \mathcal{R})$  // Apply backbone solver
5      $E_{\text{diff}} \leftarrow (E_{\mathcal{R}} \setminus E_{\mathcal{R}_+}) \cup (E_{\mathcal{R}_+} \setminus E_{\mathcal{R}})$ 
6      $V_{\text{unstable}} \leftarrow V_{E_{\text{diff}}}$ 
7      $Y_{\text{NAR}}^P \leftarrow \mathbb{1}\{x \in V_{\text{unstable}}\}$  // NAR model labels
8      $\mathcal{Y}_{\text{NAR}} \leftarrow \mathcal{Y}_{\text{NAR}} \cup \{(P, Y_{\text{NAR}}^P)\}$ 
9      $\mathcal{K}_{\text{TR}} \leftarrow \text{DFS}(P, V_{\text{unstable}}, E_{\text{diff}})$  // Find sequences
10    foreach  $K \in \mathcal{K}_{\text{TR}}$  do
11      Obtain  $P_K$  with solution  $R_K$  and sequence  $y_K$  with Improvement
12      if  $\text{Improvement} \geq \eta_{\text{improv}}$  and with probability  $\alpha_{AC}$  then
13         $\mathcal{Y}_{\text{AR}} \leftarrow \mathcal{Y}_{\text{AR}} \cup \{(P_K, y_K)\}$  // AR model labels
14      end if
15    // Skip sequences with low improvement or by probability
16  end foreach
17   $\mathcal{R} \leftarrow \mathcal{R}_+$  // Update current solution
18 end for
19 end for
20 return  $\mathcal{Y}_{\text{NAR}}, \mathcal{Y}_{\text{AR}}$ 

```

---

### B.4 Inference Details

In this section, we present the pseudocode that delineates the inference processes of L2Seg-SYN (Algorithm 3), L2Seg-NAR (Algorithm 4), and L2Seg-AR (Algorithm 5). It is important to note that our implementation leverages batch operations for efficient inference across multiple subproblems simultaneously. The K-means clustering algorithm was strategically selected for initial node identification due to its parallelization capabilities. By merging graphs from different subproblems into a unified structure, we can execute the clustering algorithm once for the entire problem space. This parallel clustering approach through K-means significantly enhances decoding efficiency. Notably, within each iterative step, our design requires only a single call of the NAR and AR models, thereby optimizing computational resources.

---

**Algorithm 3:** L2Seg-SYN: Synergized Prediction

---

**Input:** Problem  $P$ , current solution  $\mathcal{R}$ , NAR model, AR model, threshold  $\eta$ , number of clusters

**Output:** Set of unstable edges  $E_{\text{unstable}}$

```
1  $\mathcal{P}_{\text{TR}} \leftarrow \text{DecomposeIntoSubproblems}(P, \mathcal{R})$  // Partition into  $\sim |\mathcal{R}|$  subproblems
2  $E_{\text{unstable}} \leftarrow \emptyset$ 
3 for each subproblem  $P_{\text{TR}} \in \mathcal{P}_{\text{TR}}$  do
4    $\mathbf{p}^{\text{NAR}} \leftarrow \text{NARModel}(P_{\text{TR}})$  // Get NAR predictions for each node
5    $\hat{y}_{\text{NAR}} \leftarrow \{x_i \mid p_i^{\text{NAR}} \geq \eta\}$  // Identify unstable nodes via threshold
6    $\text{Clusters} \leftarrow \text{KMeans}(\hat{y}_{\text{NAR}}, n_{\text{KMEANS}})$  // Group unstable nodes into clusters
7    $\text{InitialNodes} \leftarrow \{x \mid x = \arg \max_{x_i \in c} p_i^{\text{NAR}}, c \in \text{Clusters}\}$ 
8   // Select initial node with highest probability for the AR model
9    $E_{\text{unstable}}^{P_{\text{TR}}} \leftarrow \emptyset$  // Unstable edges for this subproblem
10  for each node  $x_{\text{init}} \in \text{InitialNodes}$  with corresponding  $P_{\text{TR}}$  do
11     $E_{x_{\text{init}}}^{P_{\text{TR}}} \leftarrow \text{ARModel}(P_{\text{TR}}, x_{\text{init}})$  // Get unstable edges via the AR model
12     $E_{\text{unstable}}^{P_{\text{TR}}} \leftarrow E_{\text{unstable}}^{P_{\text{TR}}} \cup E_{x_{\text{init}}}^{P_{\text{TR}}}$ 
13  end for
14   $E_{\text{unstable}} \leftarrow E_{\text{unstable}} \cup E_{\text{unstable}}^{P_{\text{TR}}}$  // Aggregate unstable edges
15 end for
16 return  $E_{\text{unstable}}$ 
```

---

---

**Algorithm 4:** L2Seg-NAR: Non-Autoregressive Prediction

---

**Input:** Problem  $P$ , current solution  $\mathcal{R}$ , NAR model, threshold  $\eta$

**Output:** Set of unstable edges  $E_{\text{unstable}}$

```
1  $\mathcal{P}_{\text{TR}} \leftarrow \text{DecomposeIntoSubproblems}(P, \mathcal{R})$  // Partition into  $\sim |\mathcal{R}|$  subproblems
2  $E_{\text{unstable}} \leftarrow \emptyset$ 
3 for each subproblem  $P_{\text{TR}} \in \mathcal{P}_{\text{TR}}$  do
4    $\mathbf{p}^{\text{NAR}} \leftarrow \text{NARModel}(P_{\text{TR}})$  // Get NAR predictions for each node
5    $\hat{y}_{\text{NAR}} \leftarrow \{x_i \mid p_i^{\text{NAR}} \geq \eta\}$  // Identify unstable nodes via threshold
6    $E_{\text{unstable}}^{P_{\text{TR}}} \leftarrow \{(x_i, x_j) \mid x_i \in \hat{y}_{\text{NAR}} \text{ or } x_j \in \hat{y}_{\text{NAR}}, \text{ and } (x_i, x_j) \in E_{P_{\text{TR}}}\}$ 
7   // Mark all edges connected to the unstable nodes as unstable
8    $E_{\text{unstable}} \leftarrow E_{\text{unstable}} \cup E_{\text{unstable}}^{P_{\text{TR}}}$  // Aggregate unstable edges
9 end for
10 return  $E_{\text{unstable}}$ 
```

---

## C Experimental and Implementation Details

### C.1 Backbone solvers

**LKH-3.** The Lin-Kernighan-Helsgaun algorithm (LKH-3) [7] represents a strong classical heuristic solver for routing problems, which is widely used in NCO for benchmark. It employs sophisticated  $k$ -opt moves and effective neighborhood search strategies. For our experiments, we impose time limits rather than local search update limits: 150s and 240s for large-capacity CVRP2k and CVRP5k, respectively, and 2m, 4m, and 10m for VRPTW1k, VRPTW2k, and VRPTW5k, respectively. For small-capacity CVRPs, we adopt the results reported in [26].

**LNS.** Local Neighborhood Search (LNS) [9] is a powerful decomposition-based metaheuristic that iteratively improves solutions by destructively and constructively exploring defined search neighborhoods. We implement LNS following the approach in [4], where neighborhoods consisting of three adjacent subroutes are randomly selected for re-optimization. We establish time limits of 150s and 240s for large-capacity CVRP2k and CVRP5k, respectively; 2.5m, 4m, and 5m for small-capacity CVRP1k, CVRP2k, and CVRP5k, respectively; and 2m, 4m, and 10m for VRPTW1k, VRPTW2k, and VRPTW5k, respectively. LKH-3 serves as the backbone solver with a 1,000 per-step local search updates limit.



---

**Algorithm 5:** L2Seg-AR: Autoregressive Prediction

---

**Input:** Problem  $P$ , current solution  $\mathcal{R}$ , AR model, number of clusters  $n_{\text{KMEANS}}$

**Output:** Set of unstable edges  $E_{\text{unstable}}$

```
1  $\mathcal{P}_{\text{TR}} \leftarrow \text{DecomposeIntoSubproblems}(P, \mathcal{R})$  // Partition into  $\sim |\mathcal{R}|$  subproblems
2  $E_{\text{unstable}} \leftarrow \emptyset$ 
3 for each subproblem  $P_{\text{TR}} \in \mathcal{P}_{\text{TR}}$  do
4   Clusters  $\leftarrow \text{KMeans}(\text{AllNodes in } P_{\text{TR}}, n_{\text{KMEANS}})$  // Cluster all nodes
5   Centroids  $\leftarrow \{\text{ComputeCentroid}(c) \mid c \in \text{Clusters}\}$ 
6   InitialNodes  $\leftarrow \{x \mid x = \arg \min_{x_i \in c} \text{Distance}(x_i, \text{centroid}_c), c \in \text{Clusters}\}$ 
7   // Select node closest to each cluster centroid for the AR model
8    $E_{\text{unstable}}^{P_{\text{TR}}} \leftarrow \emptyset$  // Unstable edges for this subproblem
9   for each node  $x_{\text{init}} \in \text{InitialNodes}$  with corresponding  $P_{\text{TR}}$  do
10     $E_{x_{\text{init}}}^{P_{\text{TR}}} \leftarrow \text{ARModel}(P_{\text{TR}}, x_{\text{init}})$  // Get unstable edges via the AR model
11     $E_{\text{unstable}}^{P_{\text{TR}}} \leftarrow E_{\text{unstable}}^{P_{\text{TR}}} \cup E_{x_{\text{init}}}^{P_{\text{TR}}}$ 
12  end for
13   $E_{\text{unstable}} \leftarrow E_{\text{unstable}} \cup E_{\text{unstable}}^{P_{\text{TR}}}$  // Aggregate unstable edges
14 end for
15 return  $E_{\text{unstable}}$ 
```

---

**L2D.** Learning to Delegate (L2D) [4] is the state-of-the-art learning-based optimization framework that integrates neural networks with classical optimization solvers to intelligently delegate subproblems to appropriate solvers. The framework employs a neural network trained to identify the most promising neighborhoods for improvement. For comparative fairness, we apply identical time limits and backbone solver configurations as used in our LNS implementation. When augmented by L2Seg, training proceeds in two stages: we first train the L2D models following the methodology in [4], then train the L2Seg model using the resulting pre-trained L2D models.

**Initial Solution Heuristics.** For both training data generation and inference, we employ the initial solution heuristic inspired by [4]. Our method partitions nodes according to their angular coordinates with respect to the depot. We begin by selecting a reference node, marking its angle as 0, and incrementally incorporate additional nodes into the same group until the collective demand approaches the capacity threshold ( $\alpha_{\text{init}} K_{\text{veh}} C \approx \sum d_i$ ), where approximately  $K_{\text{veh}}$  vehicles would be required to service the group. This process continues sequentially, forming new groups until all customers are assigned. Finally, we apply LKH-3 in parallel to solve each subproblem independently. In our implementation, we set  $K_{\text{veh}} = 6$  and  $\alpha_{\text{init}} = 0.95$  as the controlling parameters.

## C.2 Baselines

In this section, we provide further clarification regarding the baselines used in our comparative analysis, beyond the backbone solvers. We independently executed LKH-3, LNS, and L2D using consistent parameters. Results for SIL were sourced from [5], L2R from [42], and all other baselines from [26]. When multiple variants of a baseline were presented in the original publications, we selected the configuration that achieved the best objective values.

It is important to note that all reported results were evaluated on identical test instances (for CVRPs) or on instances sampled from the same distribution (for VRPTWs), ensuring fair comparison. Moreover, our experiments were conducted on hardware with less powerful GPUs compared to those utilized in [5, 26, 42]. This hardware discrepancy suggests that the performance advantages demonstrated by our proposed model would likely persist or potentially increase if all methods were evaluated on identical computing infrastructure.

We re-implemented the backbone solvers and L2D [4] to ensure a fair and strong comparison. Notably, prior studies [26, 40] did not explore configurations optimized for L2D’s full potential. Specifically, they imposed overly conservative limits (e.g., only allowing 1 trail) on LKH-3 local search updates and did not supply current solution information to the LKH-3 solver during the resolution process. This significantly weakened L2D’s performance in their benchmarks. In contrast, our comparison reflects L2D’s best achievable performance.

### C.3 Instance Generation

In general, we generate all training and test instances following established methodologies: Zheng et al. [26] for CVRP and Solomon [52] for VRPTW. Specifically, For small-capacity CVRPs, nodes are uniformly distributed within the  $[0, 1]$  square, with integer demands ranging from 1 to 9 (inclusive). Vehicle capacities are set to  $C = 200, 300$ , and  $300$  for problem sizes 1k, 2k, and 5k, respectively. For large-capacity CVRPs, we maintain identical configurations except for increased vehicle capacities of  $C = 500$  and  $1000$  for CVRP1k and CVRP5k, respectively. For VRPTWs, we adopt the same spatial distribution, demand structure, and capacity constraints as the small-capacity CVRPs. Service times are uniformly set to 0.2 time units for each customer and 0 for the depot. Time windows are generated according to the methodology outlined in Solomon [52].

Our experimental framework comprises distinct datasets for training, validation, and testing:

- **Training:** 1,000 instances for each problem type and scale to generate training labels
- **Validation:** 30 instances per problem configuration
- **Testing:** For small-capacity CVRPs, we utilize the 1,000 test instances from Zheng et al. [26]; for large-capacity CVRPs and VRPTWs, we evaluate on 100 instances sampled from the same distribution as the training data

### C.4 Parameters and Training Hyperparameters

**Parameters.** Table 8 lists the values of parameters used in training data generation and inference. **Training Hyperparameters.** For model training, we optimize both NAR and AR architectures using

Table 8: A list of parameters and their values used in our experiments for training and inference.

Training Data Generation	
Parameter	Value
# of instances $N_{\mathcal{P}}$	1000
# of iterative steps $T_{IS}$	40
Improvement threshold $\eta_{\text{improv}}$	0
Sample coefficient $\alpha_{AC}$	0 for small-capacity CVRPs and VRPTWs 0.4 for large-capacity CVRPs
Inference	
Parameter	Value
Threshold $\eta$ for NAR model	0.6
# of K-MEANS clusters $n_{\text{KMEANS}}$	3
# of LKH-3 local search updates limit per iterative step	1000
Solve time limits	150s, 240s for large-capacity CVRP2k, 5k 2.5m, 4m, 5m for small-capacity CVRP1k, 2k, 5k 2m, 4m, 10m for VRPTW1k, 2k, 5k

the ADAM optimizer with a consistent batch size of 128 across 200 epochs for all problem variants. The learning rate is calibrated at  $10^{-3}$  for large-capacity CVRPs and  $10^{-4}$  for small-capacity CVRPs and VRPTWs. The loss function employs weighted components with  $w_{\text{pos}} = 9$ ,  $w_{\text{insert}} = 0.8$ , and  $w_{\text{delete}} = 0.2$ . All computational experiments are conducted on a single NVIDIA V100 GPU, with training duration ranging from approximately 0.5 to 1.5 days, scaling with problem dimensionality.

Regarding network architecture, our encoder maps node features  $\mathbf{X} \in \mathbb{R}^{n \times 25}$  for standard problems ( $\mathbf{X} \in \mathbb{R}^{n \times 28}$  for VRPTWs) to node embeddings via  $\mathbf{h}_i^{\text{init}} = \text{Concat}(\mathbf{h}_i^{\text{MLP}}, \mathbf{h}_i^{\text{POS}}) \in \mathbb{R}^{2d_h}$ , where  $d_h = 128$ . They then undergo processing through  $L_{\text{TFM}} = 2$  Transformer layers [47] with route-specific attention masks, followed by a Graph Attention Network to derive the final node embeddings  $\mathbf{H}^{\text{GNN}}$ . The transformer implementation utilizes 2 attention heads, 0.1 dropout regularization, ReLU

activation functions, layer normalization, and feedforward dimensionality of 512. Our GNN employs a transformer convolution architecture with 2 layers ( $L_{\text{GNN}} = 2$ ) and a single attention head.

Supplementary to the specifications in Section 4, we delineate additional hyperparameters for our decoder modules. The NAR decoder computes  $\mathbf{p}^{\text{NAR}}$  (node instability probabilities) via an MLP with sigmoid activation for final probability distribution. The AR decoder incorporates single-layer Gated Recurrent Units (GRUs), complemented by a single-layer/single-head transformer for the deletion mechanism and a four-layer/single-head transformer for the insertion procedure.

All the training hyperparameters are summarized in Table 9.

Table 9: A list of hyperparameters and their values used in our model architecture and training.

Training Configuration	
Parameter	Value
Optimizer	ADAM
Batch size	128
# of epochs	200
Learning rates	$10^{-3}$ for large-capacity CVRPs $10^{-4}$ for small-capacity CVRPs and VRPTWs
Weight of unstable nodes $w_{\text{pos}}$	9
Weight of prediction in insert stage $w_{\text{insert}}$	0.8
Weight of prediction in delete stage $w_{\text{delete}}$	0.2
Computing Resource	Single NVIDIA V100 GPU
Model Architecture	
Parameter	Value
Hidden dimension	128
<b>Encoder Transformer</b>	
# of layers $L_{\text{TFM}}$	2
# of attention heads	2
Dropout regularization	0.1
Activation function	ReLU
Feedforward dimension	512
Normalization	Layer normalization
<b>Encoder GNN</b>	
Architecture	Transformer Convolution Network
# of layers $L_{\text{GNN}}$	2
# of attention heads	1
<b>Decoder Components</b>	
NAR decoder activation function	Sigmoid
# of layers in GRUs	1
<b>AR Transformer in Deletion Stage</b>	
# of layers $L_{\text{delete}}^{\text{MHA}}$	1
# of attention heads	1
<b>AR Transformer in Insertion Stage</b>	
# of layers $L_{\text{insert}}^{\text{MHA}}$	4
# of attention heads	1

### C.5 Training Data Construction for the AR Model

We illustrate the dataset construction process for training the AR model in Figure 10. After employing backbone solvers as lookahead solvers to re-optimize the routing problems, we identify two sets of edge modifications: deleted edges ( $E_{\mathcal{R}} \setminus E_{\mathcal{R}_+}$ ), represented by blue and green dashed lines, and

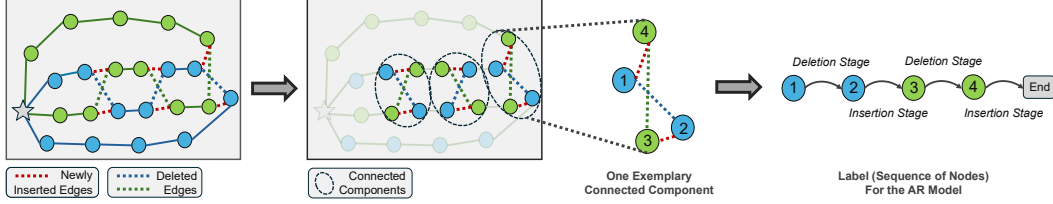


Figure 10: Training data construction process for the AR model. The process begins with edge modifications identified after re-optimization: deleted edges (blue and green dashed lines) and newly inserted edges (red dashed lines). Connected components are formed from these modified edges (shown in dashed circles). For each connected component, a depth-first search generates a node sequence alternating between deletion and insertion stages, with edges treated as undirected to allow operations from either endpoint. The node sequence serves as a training label for the AR model, terminated by an end token.

inserted edges ( $E_{\mathcal{R}_+} \setminus E_{\mathcal{R}}$ ), represented by red dashed lines. The set  $E_{\text{diff}}$  encompasses all such modified edges. Subsequently, we identify the connected components induced by  $E_{\text{diff}}$ , as shown within the dashed circles. For each connected component, we perform a depth-first search to generate a node sequence that alternates between connections via deleted edges (corresponding to the deletion stage) and inserted edges (corresponding to the insertion stage). During the depth-first search, all edges are treated as undirected, meaning the label for each stage (insertion or deletion) can originate from either endpoint. This sequence serves as a training label for the AR model and is terminated with a special end token to indicate the completion.

## D Additional Experiments and Analysis

### D.1 Hyperparameter Study

Figure 11 depicts the effects of  $n_{\text{KMEANS}}$  and  $\eta$ . We observe that the best performance is when  $n_{\text{KMEANS}} = 3$  and  $\eta = 0.6$ , suggesting that designating a moderate proportion of edges as unstable represents the most effective strategy.

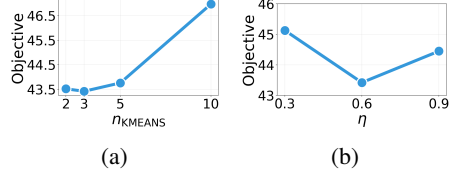


Figure 11: Analysis of key hyperparameters: (a) number of clusters  $n_{\text{MEANS}}$ , and (b) balancing factor  $\eta$ .

### D.2 Results on Realistic Routing Datasets

We further evaluate L2Seg on the CVRPLib realistic routing dataset [56, 57], adhering to the settings established in [26], which incorporates instances from CVRP Set-X [54] and the very large-scale CVRP dataset Set-XXL in the test set. The instances within CVRPLib exhibit more realistic spatial distributions (distinct from simplistic uniform or clustered patterns), greater diversity, and better representation of real-world logistical challenges. For this evaluation, we employ models trained on synthetic small-capacity CVRP2k and CVRP5k datasets and zero-shot transfer them to CVRPLib. Time constraints of 240s and 600s are implemented for L2Seg during testing. Additional methodological details are provided in Appendix C. As demonstrated in Table 10, LNS augmented with L2Seg-SYN surpasses all other learning-based methods in performance. Significantly, the computational time required by LNS+L2Seg-SYN (600s) is substantially less than that of the previously best-performing learning-based model, UDC- $\mathbf{x}_{250}$ . These results further substantiate L2Seg’s exceptional generalizability across varied problem distributions.

### D.3 Standard Deviation Comparison

In this section, we provide standard deviation statistics for L2Seg-SYN across three different backbone solvers on large-capacity CVRPs. We conduct 5 independent trials using different random seeds for each method. All experiments are terminated at the specified time limit, and we report the standard deviations of the objective values for all 6 methods. The results are presented in Table 11. While LKH-3 exhibits the lowest variance among baseline methods, our L2Seg approach also demonstrates

Table 10: CVRPLib results. We present the gap to the best known solutions (%).

Dataset, $N \in$	LEHD	ELG aug $\times 8$	GLOP-LKH3	TAM(LKH3)
Set-X,(500,1,000]	17.4%	7.8%	16.8%	9.9%
Set-XXL,(1,000,10,000]	22.2%	15.2%	19.1%	20.4%
Dataset, $N \in$	UDC- $x_2$	UDC- $x_{250}$	LNS+L2Seg-SYN (240s)	LNS+L2Seg-SYN (600s)
Set-X,(500,1,000]	16.5%	7.1%	7.5%	6.9%
Set-XXL,(1,000,10,000]	31.3%	13.2 %	12.5%	12.0%

consistently low variance across different problem types and backbone solvers, confirming both the effectiveness and stability of our method.

Table 11: Performance comparison of backbone solvers with and without L2Seg-SYN on large-scale CVRP instances. Results represent mean objective values  $\pm$  standard deviation across 5 independent trials of testing. L2Seg-SYN demonstrates consistent performance improvements with low variance, indicating both effectiveness and stability of the approach.

Methods	CVRP2k			CVRP5k		
	Obj. $\downarrow$	Gain $\uparrow$	Time $\downarrow$	Obj. $\downarrow$	Gain $\uparrow$	Time $\downarrow$
LKH-3 [7]	45.24 $\pm$ 0.17	0.00%	152s	65.34 $\pm$ 0.29	0.00%	242s
LKH+L2Seg-SYN	43.92 $\pm$ 0.20	2.92%	152s	64.12 $\pm$ 0.34	1.87%	248s
LNS [9]	44.92 $\pm$ 0.24	0.00%	154s	64.69 $\pm$ 0.37	0.00%	246s
LNS+L2Seg-SYN	43.42 $\pm$ 0.22	3.34%	152s	63.94 $\pm$ 0.35	1.16%	241s
L2D [4]	43.69 $\pm$ 0.21	0.00%	153s	64.21 $\pm$ 0.32	0.00%	243s
L2D+L2Seg-SYN	43.35 $\pm$ 0.23	0.78%	157s	63.89 $\pm$ 0.34	0.50%	248s

#### D.4 Case Study: Comparison of Predictions of Three L2Seg Approaches

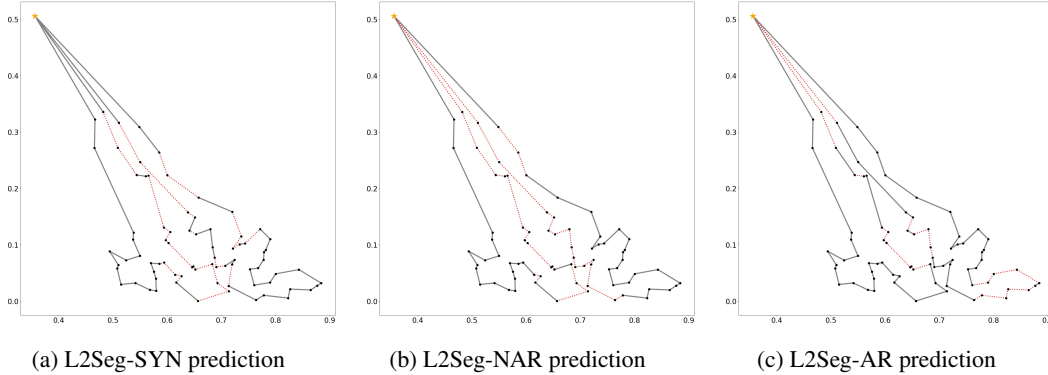


Figure 12: Prediction comparison of L2Seg-SYN, L2Seg-NAR, and L2Seg-AR on two adjacent routes from a small-capacity CVRP1k solution. Red dashed lines indicate predicted unstable edges. L2Seg-SYN provides the most reasonable predictions, while L2Seg-NAR over-predicts unstable edges and L2Seg-AR fails to identify unstable regions.

We present a case study on a small-capacity CVRP1k instance to analyze model prediction behavior. Since the learned model ultimately predicts on two adjacent routes, we visualize unstable edge predictions (red dashed lines) for two such routes using L2Seg-SYN, L2Seg-NAR, and L2Seg-AR in Figure 12. L2Seg-SYN demonstrates selective prediction behavior, avoiding boundary edges while targeting specific unstable edges within route interiors—a pattern consistent with our observations in Appendix A.1.1. L2Seg-NAR successfully identifies unstable regions (route interiors) but lacks discrimination, predicting nearly all edges within these regions as unstable without capturing local dependencies. L2Seg-AR exhibits selective prediction within regions but fails to properly identify

unstable regions, as many predictions occur at boundaries. These results provide insight into L2Seg-SYN’s hybrid approach: the NAR component first identifies unstable regions, while the AR component leverages local information to make accurate predictions within each identified region.

## **E Code Availability and Licenses**

**Our complete implementation will be made publicly available on GitHub under the MIT License upon acceptance of this paper.** All assets utilized in our research are properly attributed, and we have included licensing information as below:

1. MIT License: HGS [8], UDC [26], SIL [5], L2R [42], L2D [4]
2. Available for academic use: LKH-3 [7],  
CVRPLib (<http://vrp.galgos.inf.puc-rio.br/index.php/en/>)

## **F Broader Impacts**

On one hand, the integration of deep learning into discrete optimization offers promising advances for real-world domains such as public logistics and transportation systems, where additional considerations for social equity and environmental sustainability can be incorporated. On the other hand, the application of deep learning methodologies in discrete optimization necessitates substantial computational resources for model training, potentially leading to increased energy consumption and carbon emissions. The quantification and mitigation of these environmental impacts represent critical areas for ongoing research and responsible implementation.